ENERGY

SAN/1164-1

EVALUATION OF SELECTED DRIVE COMPONENTS FOR A FLYWHEEL POWERED COMMUTER VEHICLE

Phase I, Final Report

June 30, 1977

Work Performed Under Contract No. EY-76-C-03-1164

LMC Corporation
Sparks, Nevada

U. S. DEPARTMENT OF ENERGY

Division of Transportation Energy Conservation

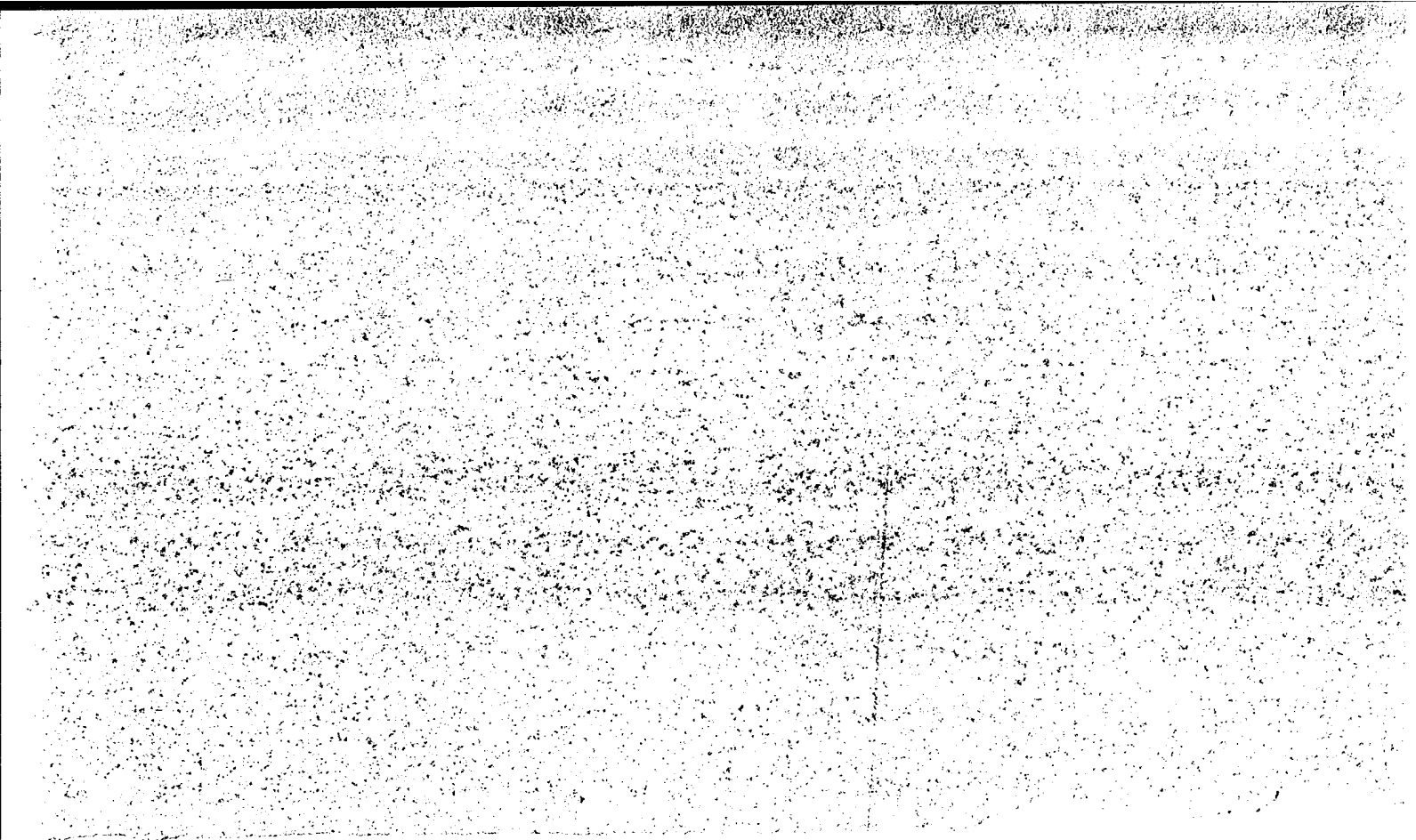

-- ((ENTER NEXT COMMAND))

*MSG DI4 DROLS PROCESSING - LAST INPUT IGNORED

*MSG DI4 DROLS PROCESSING-LAST INPUT IGNORED

*MSG DI4 DROLS PROCESSING - LAST INPUT IGNORED

-- 1 OF 1
-- ***DTIC DOES NOT HAVE THIS ITEM***
-- 1 - AD NUMBER: D425898
-- 5 - CORPORATE AUTHOR: LNC CORP SPARKS NV*
-- 6 - UNCLASSIFIED TITLE: EVALUATION OF SELECTED DRIVE COMPONENTS FOR
-- A FLYWHEEL POWERED COMMUTER VEHICLE.
-- 9 - DESCRIPTIVE NOTE: FINAL REPT.,
--11 - REPORT DATE: JUN 30, 1977
--12 - PAGINATION: 66P
--14 - REPORT NUMBER: LMC-770401-B
--15 - CONTRACT NUMBER: EY-76-C-03-1164
--20 - REPORT CLASSIFICATION: UNCLASSIFIED
--21 - SUPPLEMENTARY NOTE: PHASE I.
--22 - LIMITATIONS (ALPHA): APPROVED FOR PUBLIC RELEASE; DISTRIBUTION
-- UNLIMITED. AVAILABILITY: NATIONAL TECHNICAL INFORMATION SERVICE,
-- SPRINGFIELD, VA. 22161. SAN/1164-1.
--33 - LIMITATION CODES: 1
--*******

LMC-770401-B

SAN/1164-1
Distribution Categories UC-94b and UC-96

FINAL REPORT

EVALUATION OF SELECTED DRIVE COMPONENTS FOR A FLYWHEEL POWERED COMMUTER VEHICLE

CONTRACT EY-76-C-03-1164
PHASE I

Prepared By

LMC CORPORATION
476 Dunn Circle
Sparks, NV 89431
702-358-1215

For

United States
Energy Research and Development Administration
San Francisco Operations Office

June 30, 1977

CONTENTS

ILLUSTRATIONS

ABSTRACT

This report documents the results of tests performed at LMC Corporation (formerly Lear Motors Corporation) to evaluate the performance of selected high-speed flywheel bearings and shaft seals under Contract EY-76 C-03-1164. This report also documents the work performed by U. S. Flywheels, Inc. on development of a high-speed composite flywheel rotor for this program under subcontract from LMC Corporation.

The overall program objective is to develop a composite flywheel system for primary energy storage in a flywheel powered vehicle. These initial tests were intended to evaluate the performance of full-size composite rotor elements, high-speed bearings and shaft seals for that system under conditions simulating as closely as possible those anticipated in a finished vehicle.

Performance of the angular contact ball bearings is reported to be satisfactory at all speeds; a simplified lubrication system is recommended for second generation hardware. Performance of the ferrofluidic shaft seals is reported to be marginal, as they failed to hold a hard vacuum at the maximum design speed. Several concepts for improved seals are offered for second generation hardware.

The test objectives for the high-speed composite flywheel rotor were not achieved by U. S. Flywheels, Inc. due to dynamic instability problems with the test hardware.

Recommendations are offered for the design of second generation hardware, and a scope of activities is proposed for the second phase of this program.

The total cost and fee for performance of this contract was $199,013. The original period of performance was from December 17, 1975 to September 17, 1976. This completion date was later extended to June 30, 1977 by modification to the contract.

1.0 INTRODUCTION AND PROJECT SUMMARY

This report documents work funded by the Energy Research and Development Administration (ERDA) in Phase I of Contract EY-76-C-03-1164. The contract was awarded to Lear Motors Corporation (now LMC Corporation) as a result of an unsolicited proposal (Reference 1) for development of an energy storing flywheel powerplant for a short-range commuter vehicle similar to that illustrated in Figure 1-1. The Phase I tasks funded by ERDA were directed towards evaluating and characterizing specific technologies associated with the flywheel propulsion system that were considered to be critical to the successful development of the proposed commuter car.

The vehicle flywheel would be designed to operate between 20,000 and 41,000 rpm, storing a total of 16 kw-hrs at the maximum speed of 41,000 rpm. Vertical spin axes were selected so that normal vehicle cornering would not induce gyroscopic forces on the flywheel bearings. Two rotors would turn in opposite directions so that any gyroscopic forces produced by vehicle pitch or roll motions would be balanced within the flywheel assembly and not reflected to the chassis. Each rotor would be assembled from six identical modules stacked on a common shaft, each module being of multi-rim construction similar to that shown in Figure 1-2. In Phase I, the rotor testing was to be limited to the outer (most highly stressed) rims from a single module. The bearings and seals were to be tested under load conditions simulating those expected from a complete six module rotor.

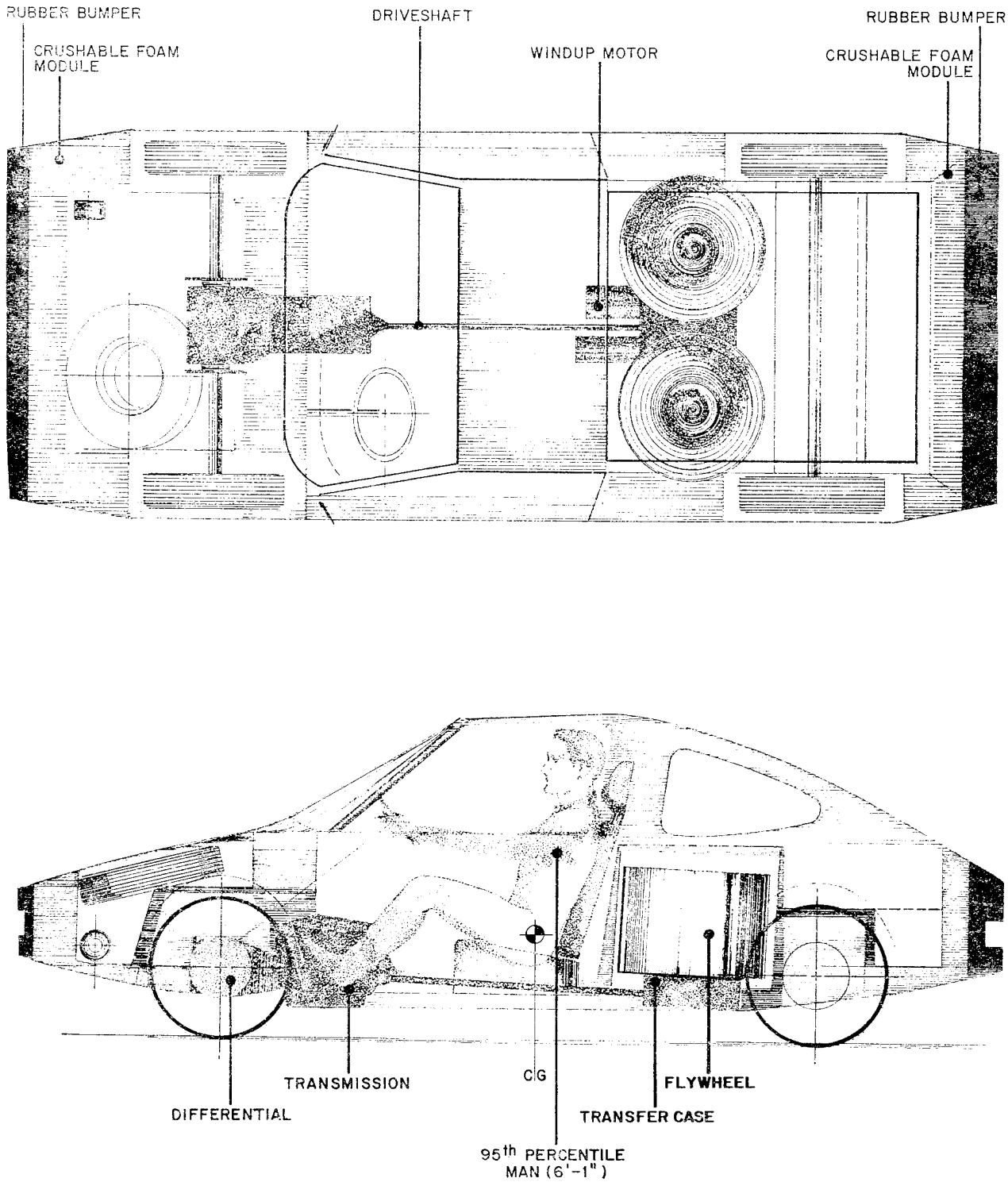

FIGURE 1-1

FLYWHEEL POWERED COMMUTER VEHICLE

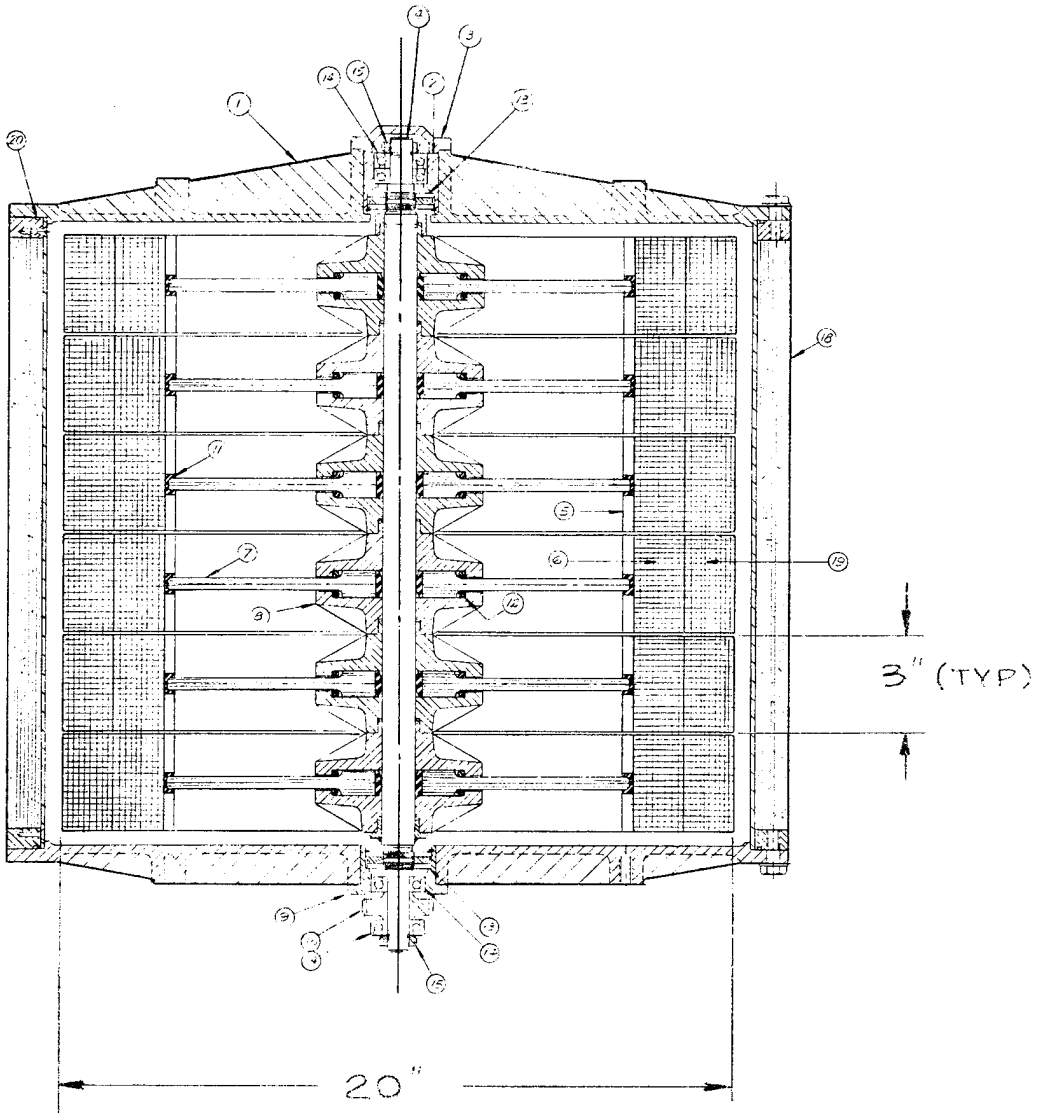

FIGURE 1-2

ORIGINAL FLYWHEEL CONCEPT - SIX MODULE CONFIGURATION

1.1 OBJECTIVES AND SCOPE

These initial tests under Phase I were intended to evaluate the performance of full-size rotor elements, bearings, and shaft seals under conditions simulating as closely as possible those anticipated in a finished vehicle. Of primary concern was the structural integrity of the composite rotor elements under the high g-forces generated at maximum speed, the combined drag torque of all three bearings and two seals on each shaft, the amount of lubricant flow required through the bearings to remove generated heat, and the ability of the seals to contain a hard vacuum at the high shaft speeds involved.

1.2 ROTOR DEVELOPMENT

Rotor development was subcontracted to U. S. Flywheels, Inc. (USFI). The contract required that two full-size rotor elements be spun to failure for the purpose of establishing a baseline energy storage capacity, and to determine the ultimate strength of the composite under centrifugal loading conditions. Although the specific goals of this portion of the program were not met, several significant accomplishments can be reported:

a) A proprietary process for wet-winding fiber-epoxy composite flywheel rims using vacuum imprenation with precision tension and positioning controls was developed and reduced to practice by USFI during the period of this contract.

b) Full size Kevlar-49 test rims weighing approximately 13 pounds each were wound with a room temperature cure flexible epoxy resin developed by USFI for this program. There was no apparent degradation in the composite due to either mechanical or thermal effects during the cure cycle. Small test rings (5.75" ID) wound with the same materials and by the same processes (conforming to ASTM Specification D2291) demonstrated ultimate strengths in excess of 250 KSI in static tension tests (performed in accordance with ASTM Method D2290).

c) Construction of a fully instrumented spin test facility was completed in the third quarter of the contract. This facility is capable of rotating rims up to 36 inches in diameter and up to 24 inches long. Rotors weighing up to 200 pounds can be spun, and speeds up to 60,000 rpm can be achieved.

Numerous attempts to spin the test rims to the anticipated burst speed of 46,000 rpm using a novel shaft-to-rim attachment mechanism designed for this purpose by USFI were unsuccessful. The maximum speed reported was approximately 10,000 rpm, the limitation being a dynamic instability of the spoke-rim system at that speed.

1.3 BEARINGS AND SEALS DEVELOPMENT

Spin tests of flywheel bearings and shaft seals were conducted at LMC Corporation under full load conditions at speeds up to the design maximum of 41,000 rpm. Drag torque and temperature rise measurements were made continuously during these tests. Vacuum integrity of the seals was monitored during portions of the test program.

Performance of the angular contact ball bearings was satisfactory, however the original pressurized oil-jet lubrication system was found to deliver excessive quantities of lubricant. A wick feed air-oil mist lubrication system is proposed for second generation hardware.

Performance of the "centrifugal" ferrofluidic seals was unsatisfactory as they did not withstand adequate pressure differentials although their drag torque was quite low. Performance of the "conventional" ferrofluidic seals was marginal. Their drag torque was acceptable, however their sealing integrity above 38,000 rpm was inadequate.

For second generation hardware, a unitized bearing/seal cartridge is proposed. This would combine a duplex pair of bearings and a

hybrid seal on a short hollow shaft with a self-contained wick feed or magnetic fluid lubrication system to simplify assembly, increase shaft rigidity, and permit better control of critical seal clearances. Such hardware should produce better sealing integrity and lower parasitic losses over the entire speed range.

1.4 CONCLUSIONS AND RECOMMENDATIONS

The rotor development program did not meet contractal objectives because dynamic instability problems with the test apparatus would not permit full speed operation in USFI's test facility. An analysis of the rotor dynamics problem is presented in Appendix B to this report. The source of the difficulty is believed to be in the design of the novel shaft-to-rim attachment mechanism used in these tests. A completely different approach is recommended for second generation hardware. The most promising design known to LMC Corporation at this time is the "tension balanced spoke" concept presented by William M. Brobeck & Associates in their published report EPRI EM-227 (Reference 7). It is recommended that such a system be developed in Phase II of this program.

The bearings and seals program did partially fulfill the contractual objectives in that full speed testing was completed under full load conditions. Problems were discovered with the seals, however solutions appear to be available. It also appears that the bearing lubrication system can be simplified, and additional testing of second generation hardware is recommended.

Also recommended is that Phase II be redirected to focus on development of a single-module, single-rim flywheel system, complete with containment structure and vacuum system, for use in hybrid powerplants. These could then become workhorse units available to other ERDA contractors for integration into all manner of hybrid powerplants. Details are presented in Section 5.0 of this report.

2.0 ROTOR PROGRAM

All rotor elements developed for this program were composite rings filament wound from Kevlar-49 fiber. Fiber volumes were in the range of 70 to 75%. Ultimate composite tensile strengths under centrifugal loading were expected to be in the range of 280 to 285 ksi. Dimensions of the highly stressed outer elements originally proposed for the vehicle flywheel system were:

Inside diameter	17 inches
Outside diameter	20 inches
Axial length	3 inches
Approximate weight	13 pounds

At the maximum design speed of 41 krpm, these elements would see a maximum hoop tensile stress of approximately 227 ksi, a maximum tensile radial stress of approximately 2 ksi, and would store approximately 838 watt-hours of kinetic energy (64.5 watt-hours per pound). Burst speed was expected to be in the neighborhood of 46 krpm (285 ksi and 81.1 watt-hours per pound). In order to achieve the highest possible hoop strengths, all rims were wound from 1420 denier yarn. Knots or broken ends were not allowed, each rim being wound from continuous yarn.

An in-house development program was underway at USFI at the time the contract for this program was awarded. The purpose of the in-house program was to demonstrate dynamic stability of a multi-rim rotor having three concentric rims. The first step in that program was to develop the innermost rim and its shaft-to-rim attachment hardware. This innermost rim was to be smaller than the ERDA/LMC rim, but would be of the same Kevlar construction:

Inside diameter	13 inches
Outside diameter	14.3 inches
Axial length	3 inches
Approximate weight	4.2 pounds

At their maximum design speed of 32.5 krpm, these rims would see a maximum hoop tensile stress of approximately 70 ksi, and would store approximately 22 watt-hours per pound.

This in-house program was identified by USFI as Project "A" and the ERDA/LMC program was identified as Project "L". The two programs ran concurrently, and the test results reported in Section 2.4 includes data from both.

2.1 WINDING FACILITY DEVELOPMENT

At the beginning of this program, USFI maintained that precision winding of full-size rims for optimum hoop and radial strengths from Kevlar-49 under centrifugal loading was not an established commercial process, and development of special winding apparatus would be necessary to produce rims of sufficient quality to meet the goals of this program. However, development of such winding equipment was not included in the Statement of Work nor in the budget of this program. USFI thus developed their own in-house precision winding facility at their own cost as capital equipment. Special winding mandrels and mandrel removal tools used to produce the specific test rims and smaller NOL rings (ASTM Specification D 2291) required for this program were fabricated at Contract expense. These are reusable tools, and can be used to produce additional test rims in Phase II.

The winding machine is fairly conventional. It has a horizontal drive spindle with continuously variable speed controls. Its speed range is 0 to 200 rpm; it can produce rims up to 53 inches in diameter. The fiber traversing mechanism is electronically controlled to permit precision placement on the mandrel. The fiber tensioning device is a proprietary development of USFI which permits tension control within a few grams regardless of tension setting or winding speed. A system for vacuum impregnation of the fiber is another proprietary development of USFI.

Room temperature curing flexible epoxy systems were thought to be the most promising matrix materials because room temperature curing would minimize residual stresses due to thermal effects, and a flexible matrix would minimize radial stresses under centrifugal loading. Numerous different epoxy systems were used to fabricate NOL test rings (ASTM Specification D2291) early in the program. Most formulations were based upon DER 332 or XD7575 resins and DEH 29 (Dow Chemical Company) or Ancamine 500 or Ancamine 1656 (Pacific Anchor Chemical Company) curing agents.

The NOL rings were 0.250" wide by 0.125" thick with a 5.75" inside diameter. They were tested in accordance with ASTM Method D2290-69 to determine their static tensile strength. Wide data scatter was reported in the beginning:

TABLE 2-1

NOL RING TEST DATA

NOL RING NUMBER	DENSITY IN LBS/IN^3	% FIBER BY VOLUME	COMPOSITE STRENGTH IN KSI
1	.0430	42.3	138.7
2	.0477	57.5	206.3
3	.0442	66.8	197.0
4	.0482	70.6	152.0
5	.0462	61.04	131.1
6	.0443	60.3	164.7
7	.0457	59.5	150.5
8	.0473	64.2	63.1
9	.0485	69.3	193.9
10	.0476	--	145.9
11	.0464	--	198.9
12	.0472	60.6	200.2
13	.0500	55.44	152.6
14	.0494	59.70	173.8
15	.0522	75.3	208.8
17	.0497	61.0	193.4
21	.0426	75.0	176.2

Later in the program, USFI verbally reported NOL ring test results in excess of 250 ksi. These were wound and tested for Project "A", and tabulated data has not been submitted.

2.2 TEST FACILITY DEVELOPMENT

Construction of USFI's spin test facility was initiated at their Canoga Park facility before their participation in this program began in March of 1976. All equipment was moved to their new Irvine facility in October 1976, and installed above ground on a reinforced concrete pad surrounded by concrete walls. Installation of the compressed air supply, instrumentation, and controls was completed by November 1, 1976. This work was not included in the Contract, and was financed from USFI's capital budget. Delays in the construction and installation of this equipment were the primary cause of the repeated schedule slippage experienced between March and November of 1976.

A sketch of the vacuum spin test hardware is shown in Figure 2-1. It consists of a 42" diameter vacuum chamber with a Bendix Model PMC-6B diffusion pump and a Welch Scientific Duo-Seal roughing pump, a Barber-Stockwell Model 2501 air turbine and related drive shaft components. A lead safety barrier is positioned between the test elements and the walls to prevent damage to the chamber during spin-to-failure tests. Turbine speed control is accomplished by use of a Barbour-Stockwell Model 105-B Turbine Governor System. Test instrumentation includes digital readout and oscillographic recording of turbine speed. Proximity probes are positioned around the drive shaft, and their output, along with chamber pressure and turbine air pressure are also recorded on oscillographic recorders.

This facility was designed for an ultimate capability of spinning rims up to 36 inches in diameter and up to 24 inches long. Rotors weighing up to 200 pounds can be accommodated, and speeds up to 60,000 rpm are possible.

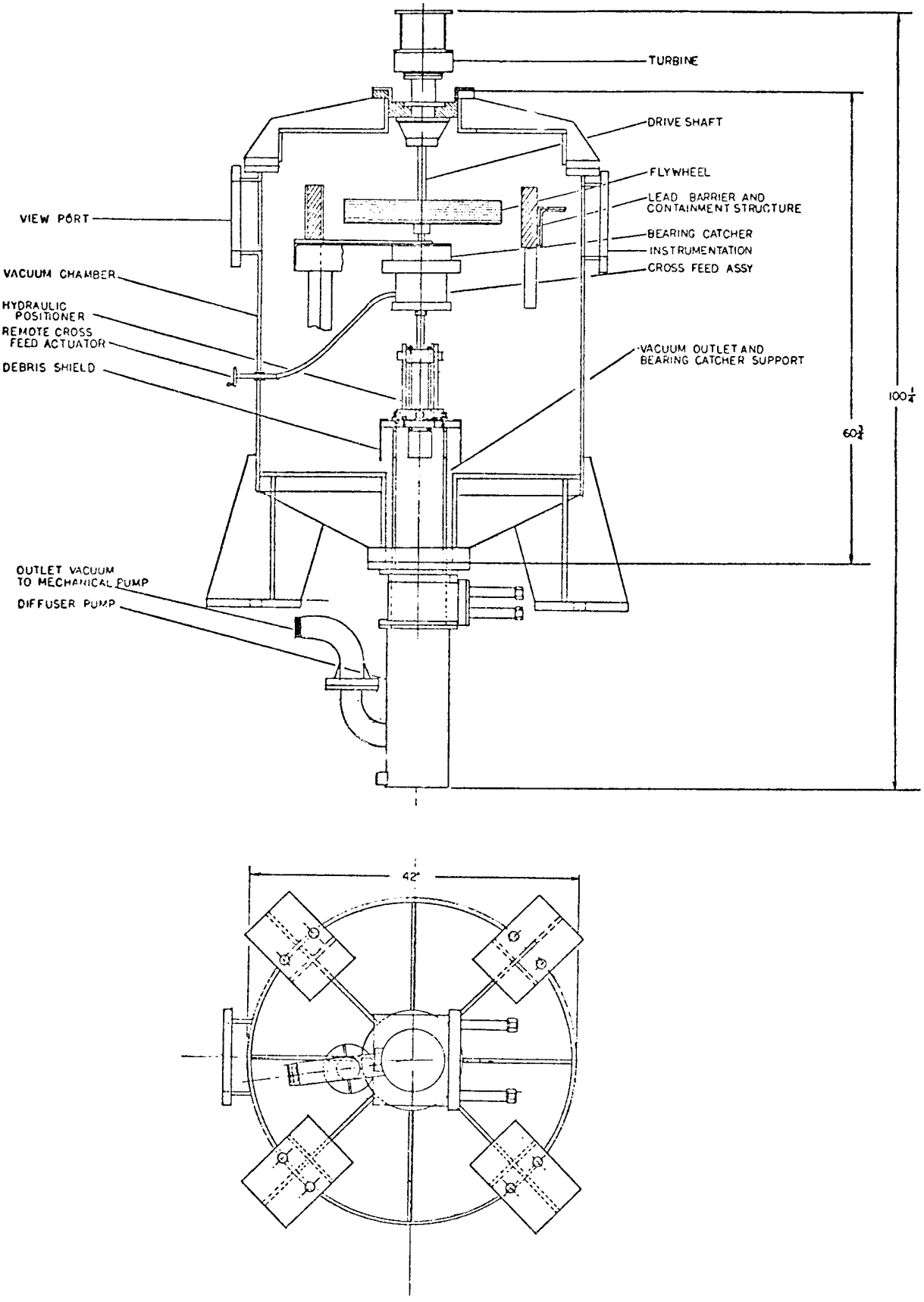

FIGURE 2-1

VACUUM SPIN TEST HARDWARE

2.3 ROTOR DESIGN

Project "L" did not require development of the final shaft-to-rim hardware during Phase I. However, some form of shaft-to-rim hardware had to be used in the laboratory in order to spin the test rims to design speeds. USFI designed a laboratory hub and spoke system for this purpose as shown in Figure 2-2. The hub and spokes were fabricated from high strength steel; each spoke attached to the rim through a novel elastic device bonded to the ID of the test rim. The design of this device was not funded by this contract and USFI considers its details proprietary. Therefore, no further description shall be given here. LMC's engineers accepted this design as adequate for laboratory testing although it did not appear to be adequate for a practical automotive system that would be exposed to externally generated forces and moments. It now appears that insufficient spoke stiffness contributed to a spin-whirl resonance at speeds far below target values, and the spoke-to-rim connection had insufficient strength to withstand the resulting forces generated therein. Post-test analysis (Appendix B) confirms that spoke stiffness and dynamic stability considerations were not adequately considered when the original hardware was designed.

2.4 TEST PROCEDURES AND RESULTS

All spin testing of full-size rims for this "L" program was to be done in accordance with Test Procedure LMC-760301-B (Reference 4), which required that each element be spun to a maximum speed of 45.9 krpm or to failure of the composite, whichever occurred first. Requirements of the "A" program were less formal; speeds, stresses, and energy levels were lower, and thus USFI elected to spin "A" hardware first.

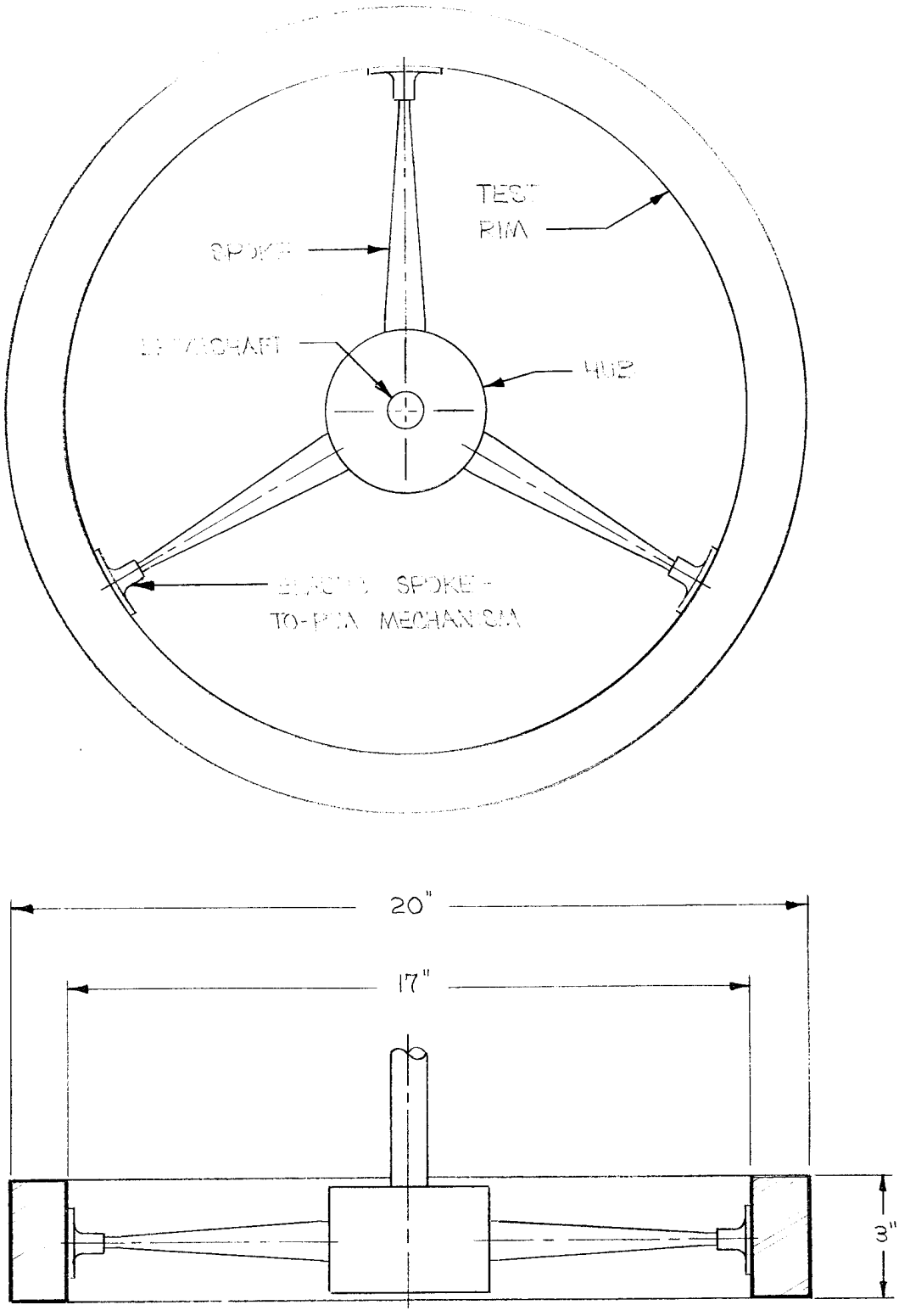

FIGURE 2-2

ROTOR TEST ELEMENT

On November 19, 1976, an attempt was made to spin the complete (A) system to its maximum test speed of 32.5 krpm. This system became dynamically unstable at approximately 4.5 krpm and was destroyed. The driveshaft was fractured; all three spokes were bent approximately 90^{o} (in their original plane of rotation) where they had engaged the spoke-to-rim cups; the cups themselves were shattered. The composite rim was cut nearly in half along a circumferential line on its inside surface in the plane in which the spokes had been located. The outer surfaces of the rim showed minor signs of abrasion where they had contacted the walls of the spin chamber. The problem was thought to be insufficient damping in the drive shaft, and changes to the test equipment were made accordingly.

On December 1, 1976, in a preliminary checkout run of the modified drive shaft, "L" system metalware (shaft, hub, and spokes but no composite rim) was spun to 44.2 krpm without difficulty.

On December 13, 1976, an attempt was made to spin the complete "L" system to 45.9 krpm. It too became dynamically unstable and was destroyed at approximately 4.05 krpm. The mode of failure was similar to that observed earlier with the "A" system.

Subsequent testing of modified "A" system and "L" system components resulted in gradual improvements up until the "L" program was terminated in March of 1977. The maximum speed reported on a complete "L" system at that time was approximately 10 krpm, the limiting factor being a gross instability at that speed. The maximum speed reported on a complete "A" system was 32.5 krpm, the design maximum. Redesign of "L" hardware in accordance with changes in the shape of the spokes and construction of the cups that proved effective with "A" hardware were undertaken, however the individual components were not finished prior to termination of the program. In all, 22 test runs were made on metalware (both programs) and 27 runs were made with complete hardware.

2.5 POST TEST ANALYSIS

Failure of the USFI flywheel system to achieve target speed prompted a review of the dynamics of pendulus rotors. A complete analysis is presented in Appendix B to this report.

The case of a pendulously mounted "rigid" hub/disk system is well known. Shaft whip is a limiting condition, and the shaft first critical frequency must be above twice the desired operating speed. The shaft critical involved is that of a clamped-free end condition due to the stabilizing effect of the disk when operating at high speed. Excitation for the shaft whip can be provided by a stable forward whirl mode resonance at twice spin speed, which yields one stress cycle in the shaft per spin revolution.

Spin-whirl maps were prepared for both "A" and "L" systems. Several interesting facts emerged when comparing theory with actual experience with the relatively "soft" hub/rim system:

a) The first critical shaft-whip frequency is definitely high enough so the failures cannot be attributed to shaft whip acting alone.

b) All of the failures occurred during passage of the two-times-spin forward resonance frequencies.

c) When running metalware only, no problems were encountered when passing the above frequencies.

The only plausible failure mode consistent with the above is a whip-like instability involving not only the shaft, but the shaft/hub/spoke combination. This instability is of a lower frequency than the exciting 2X spin forward whirl.

The analysis of Appendix B shows that as the 2X intersection is approached, the ratio of $\theta 1/\theta 2$ shown in Figure 2-3 (angular hub displacement/angular rim displacement) approaches zero. In other words, the coupling between rim and hub becomes soft, and spoke forces are low. This allows any hub vibration to be excited by the 2X whirl resonance. Indeed, calculations show that the hub-shaft-quill combination has an unstable $\theta 1$ motion at a frequency above the 2X spin frequency but less than the 2X whirl frequency. The added hysterisis losses in the spokes produces torsional forces on the hub to compound the already unstable vibration. The conclusion is that both stiffer spokes and proper polar ratios are needed for a stable system.

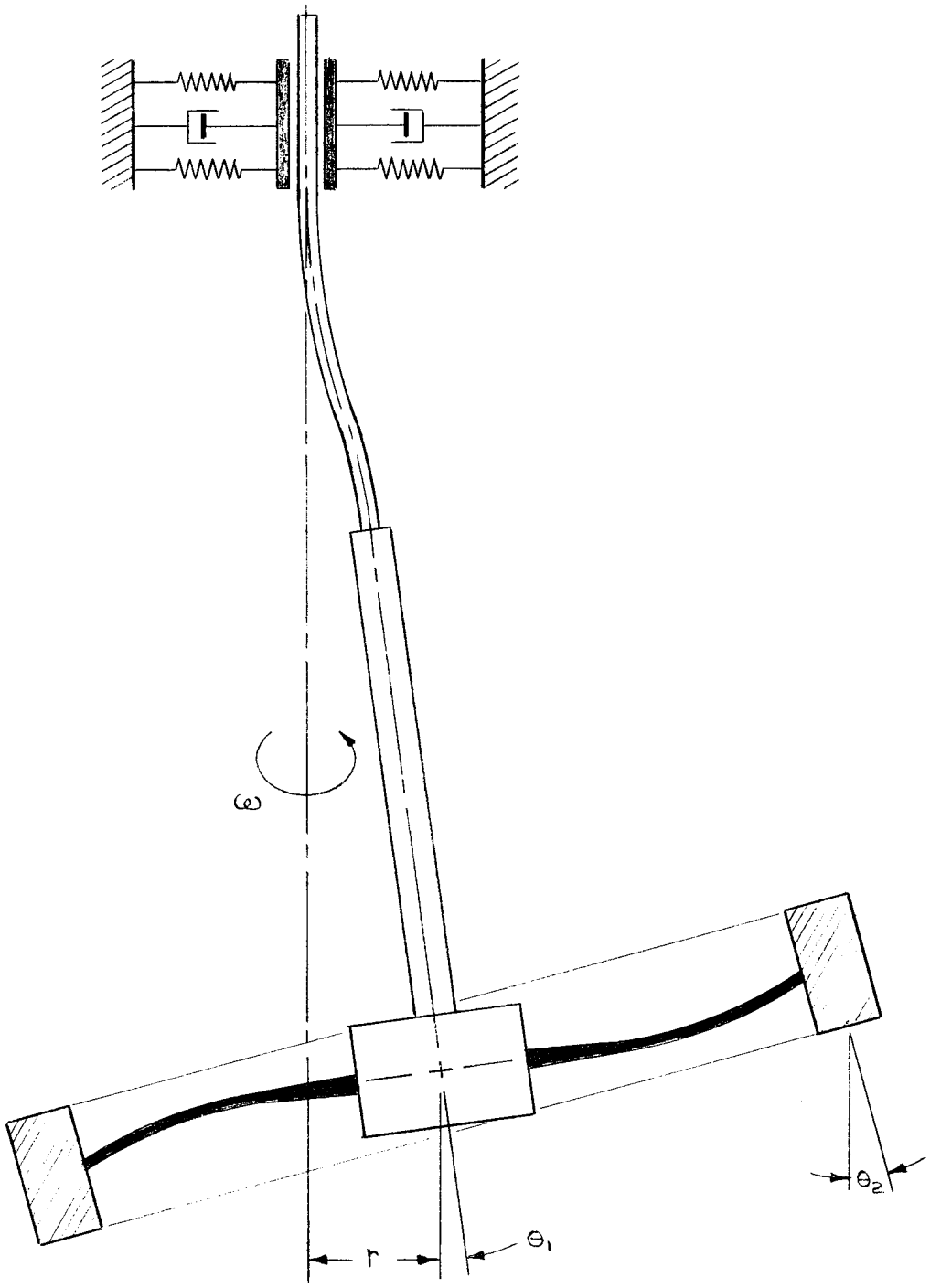

FIGURE 2-3

DYNAMIC MODEL OF TEST SYSTEM

3.0 BEARINGS AND SEALS PROGRAM

Each of the two flywheel rotors proposed for the commuter vehicle would weigh 175 pounds and spin on a vertical shaft supported by three angular contact ball bearings. Ferrofluidic shaft seals would be used between the upper and lower bearings to permit maintenance of a hard vacuum in the rotor cavity and a partial vacuum in the bearing cavities. The shaft would drive into a speed reduction unit which would probably add one additional bearing pre-loaded in the opposite direction to control axial stiffness of the entire assembly. However, since the reduction unit has not been identified, and since this fourth bearing would be smaller than the others, no attempt was made to simulate this component of the final system.

These tests were performed to evaluate the ability of these bearings and seals to function properly under the conditions anticipated in finished vehicle systems. Of primary concern was the combined drag torque of all three bearings and two seals, the amount of lubricant flow required through the bearings to remove generated heat, and the ability of the seals to contain a hard vacuum at the high shaft speeds required. Problem areas were to be identified and corrective recommendations made.

3.1 DESCRIPTION OF TEST HARDWARE

All three bearings were precision non-separable angular contact spindle bearings with phenolic retainers and fifteen degree initial contact angle. These bearings were developed specifically for high speed applications where both axial and radial loads are present. The lubricant was Monsanto's Santotrac-30, a synthetic hydrocarbon oil specifically developed for rolling contact elements under heavy loads at high speeds. Figure 3-1 illustrates the location of each bearing in the test hardware as well as details of the pressurized oil-jet lubrication system:

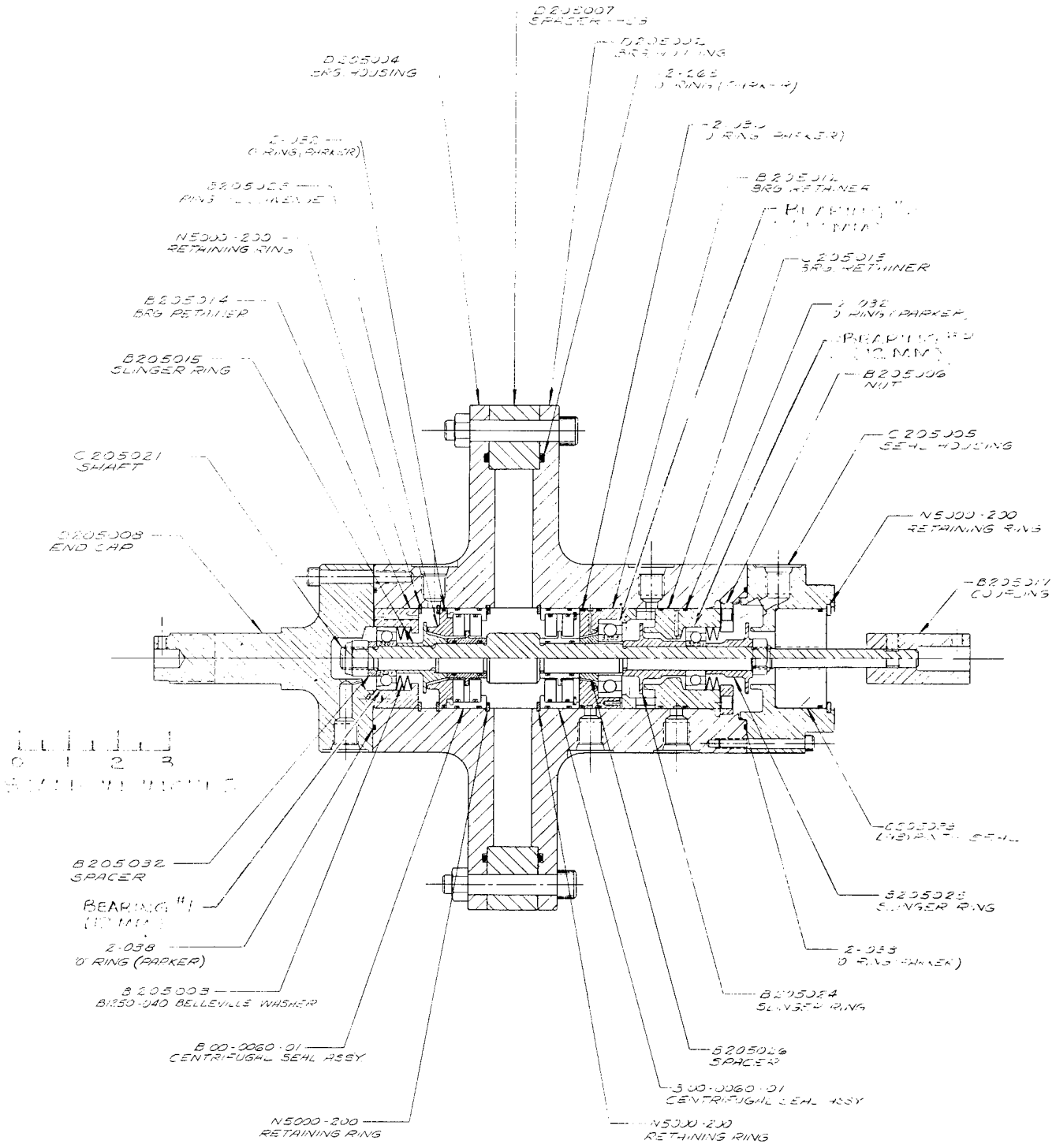

FIGURE 3-1

TEST ITEM - WITH CENTRIFUGAL SEALS

Bearing No. 1. . . . . Barden P/N 201 H (12 mm bore)
Bearing No. 2. . . . . Barden P/N 203 H (17 mm bore)
Bearing No. 3. . . . . Barden P/N 201 H (12 mm bore)

The bearings were set up to share the total thrust load of 175 pounds. Bearings No. 1 and 2 were clamped solidly to the shaft and allowed to float axially in the housing; preload springs were used against their outer races to produce a thrust load of approximately 55 pounds on each. Bearing No. 2 had its outer race clamped in the housing and thus carried the remaining 65 pounds. Bearing No. 2 was assembled with a slight radial clearance between its bore and the shaft, thus minimizing the possibility of binding due to the classic problem of misalignment in 3-bearing systems. Figure 3-2 is a photograph of the test hardware prior to assembly. Magnetic fluid seals were used to permit a hard vacuum to be maintained in the rotor cavity. Two different seal configurations were tested. Both were designed specifically for this application by Ferrofluidics Corporation:

Centrifugal test seals . . . .Ferrofluidics Dwg. 00-0060-01
Conventional test seals . . . Ferrofluidics Dwg. 11006001

Design features of the centrifugal seals are shown in Figure 3-3. These operate on the same principle as ordinary slinger seals; at design speeds, the fluid is trapped in an annular space surrounding the slinger and held there by hydrodynamic pumping forces generated by the slinger. Therefore, their ability to seal against differential pressures increases with speed. But unlike ordinary slinger units which do not maintain a hermetic seal at zero speed, the magnetic fluid in the ferrofluidic seal is held in place at zero speed by the surrounding magnet. Thus a hermetic seal is maintained, however its differential pressure capacity is limited to a few psi at zero speed. These centrifugal seals were certain to have low drag, however their sealing performance had not been verified prior to beginning this program.

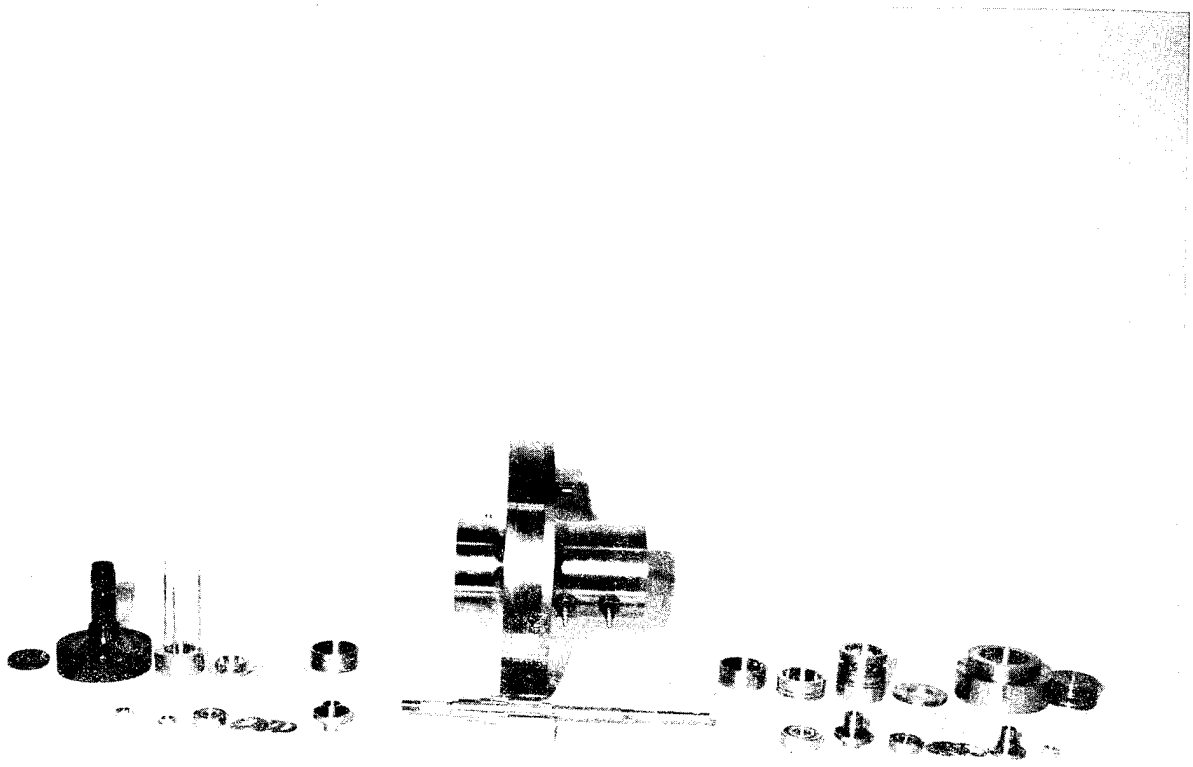

FIGURE 3-2

TEST HARDWARE PRIOR TO ASSEMBLY

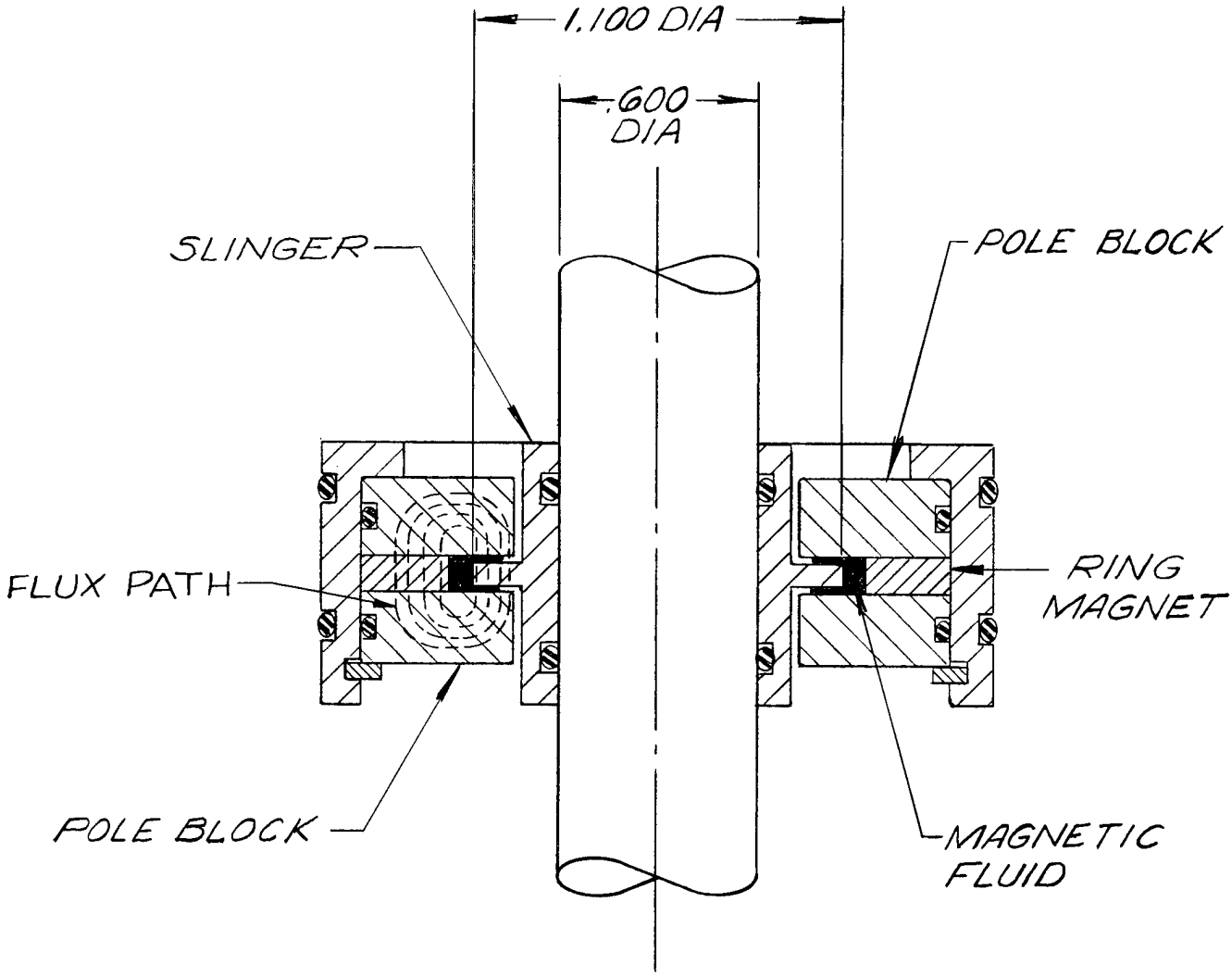

FIGURE 3-3

CENTRIFUGAL TEST SEALS

Therefore, Ferrofluidics Corporation also supplied a pair of conventional ferrofluidic seals as backup units. Design features of these conventional seals are shown in Figure 3-4. In this configuration, the pole blocks and magnet form part of a magnetic circuit that is completed by the shaft. Magnetic fields then focus and hold the magnetic liquid between the stationary and rotating surfaces as if it were a liquid O-ring. The pressure differential that the seal can withstand depends on the number of stages, each stage typically withstanding 3 to 5 psi. These conventional seals were certain to seal better than the centrifugal units at low speeds, however their drag torque was expected to be significantly higher. As a result, the fluid's temperature rise due to viscous shear at the higher speeds was identified as a potential problem.

In the original flywheel system concept, the bearings were to operate in a partial vacuum of 5 psia, and each rotor was to drive directly into a speed reduction unit which also was to operate at 5 psia. As such, the seals would only have to maintain a differential pressure of 5 psi and there would be no requirement for a high speed dynamic seal below the lower rotor bearings. In the test fixture however, a third seal, hereafter referred to as the "workhorse" seal, was required to permit maintenance of the partial vacuum in the lower bearing cavity. Two different configurations were used during the test:

Ferrofluidic workhorse seal . . . .Ferrofluidic Dwg. 11003801
Labyrinth workhorse seal . . . . . LMC Dwg. C205033

In the region of the workhorse seal, the shaft diameter was made smaller than at the test seals (0.375" vs. 0.600") to minimize drag torque of the workhorse seal. Any measurable drag resulting from the workhorse seal prior to installation of the test seals was to be subtracted from the total torque recorded thereafter.

Figures 3-5 and 3-6 illustrate the basic test setup. The test hardware itself was suspended from a test stand through a self-aligning, low

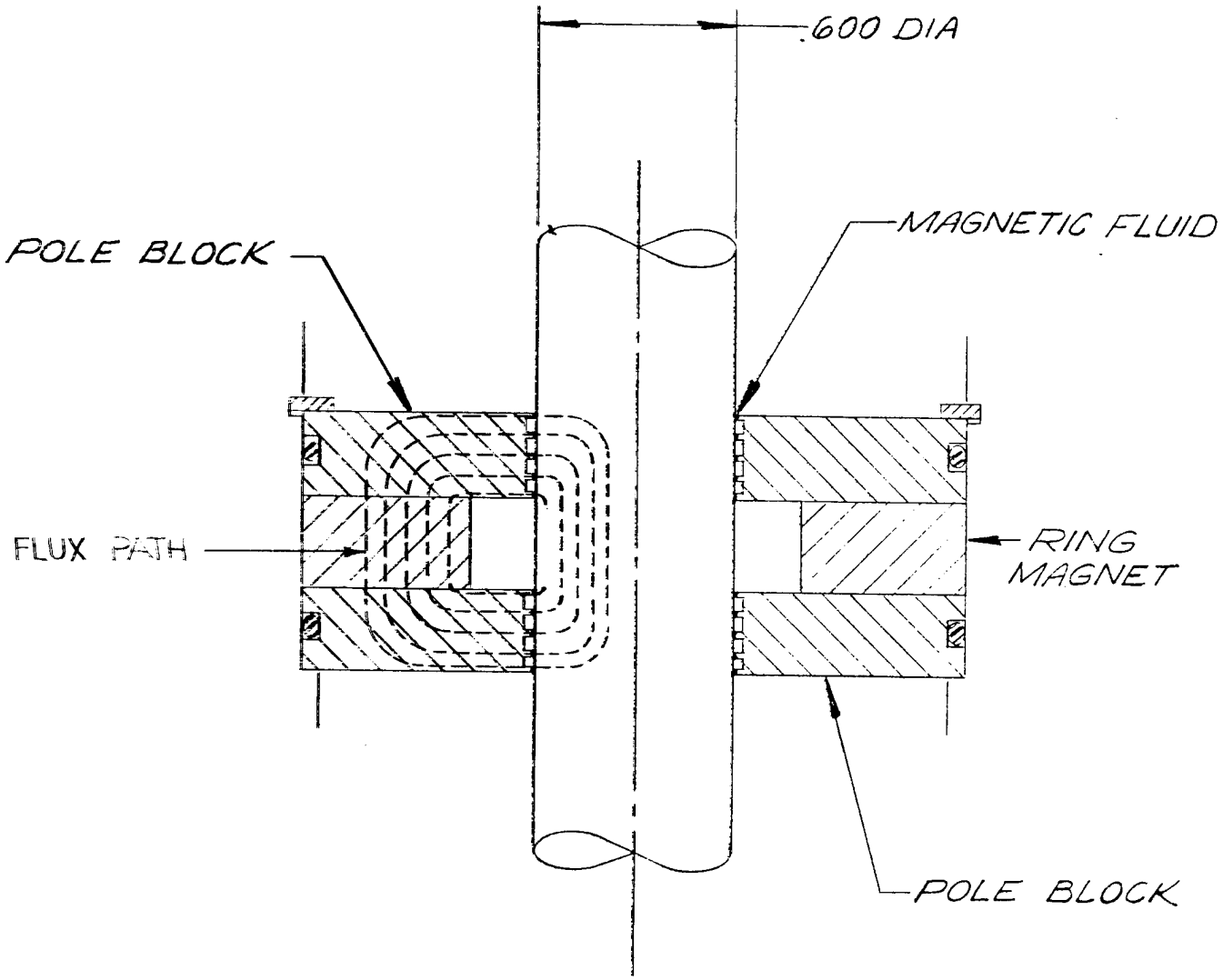

FIGURE 3-4

CONVENTIONAL TEST SEALS

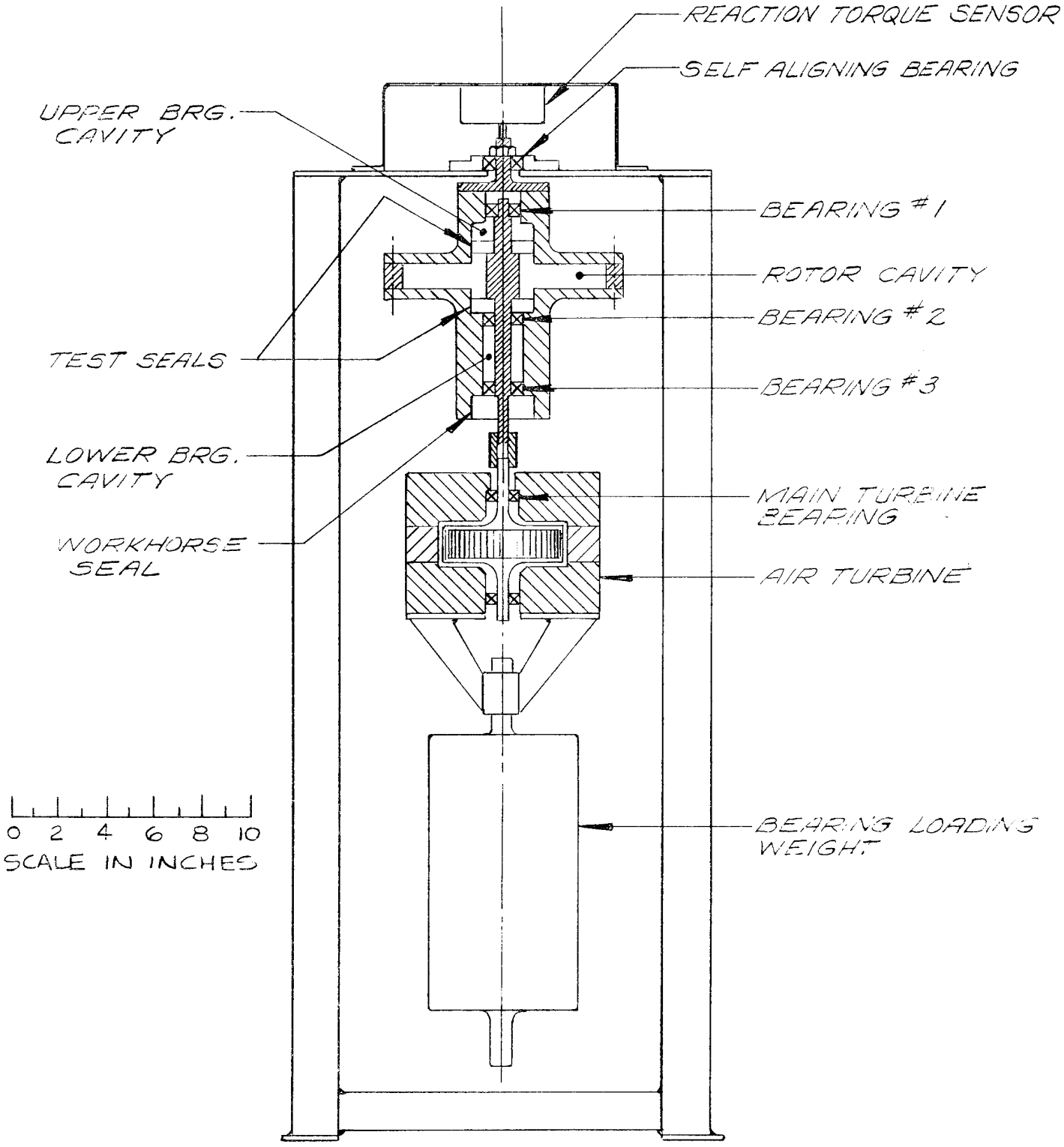

FIGURE 3-5

TEST SETUP

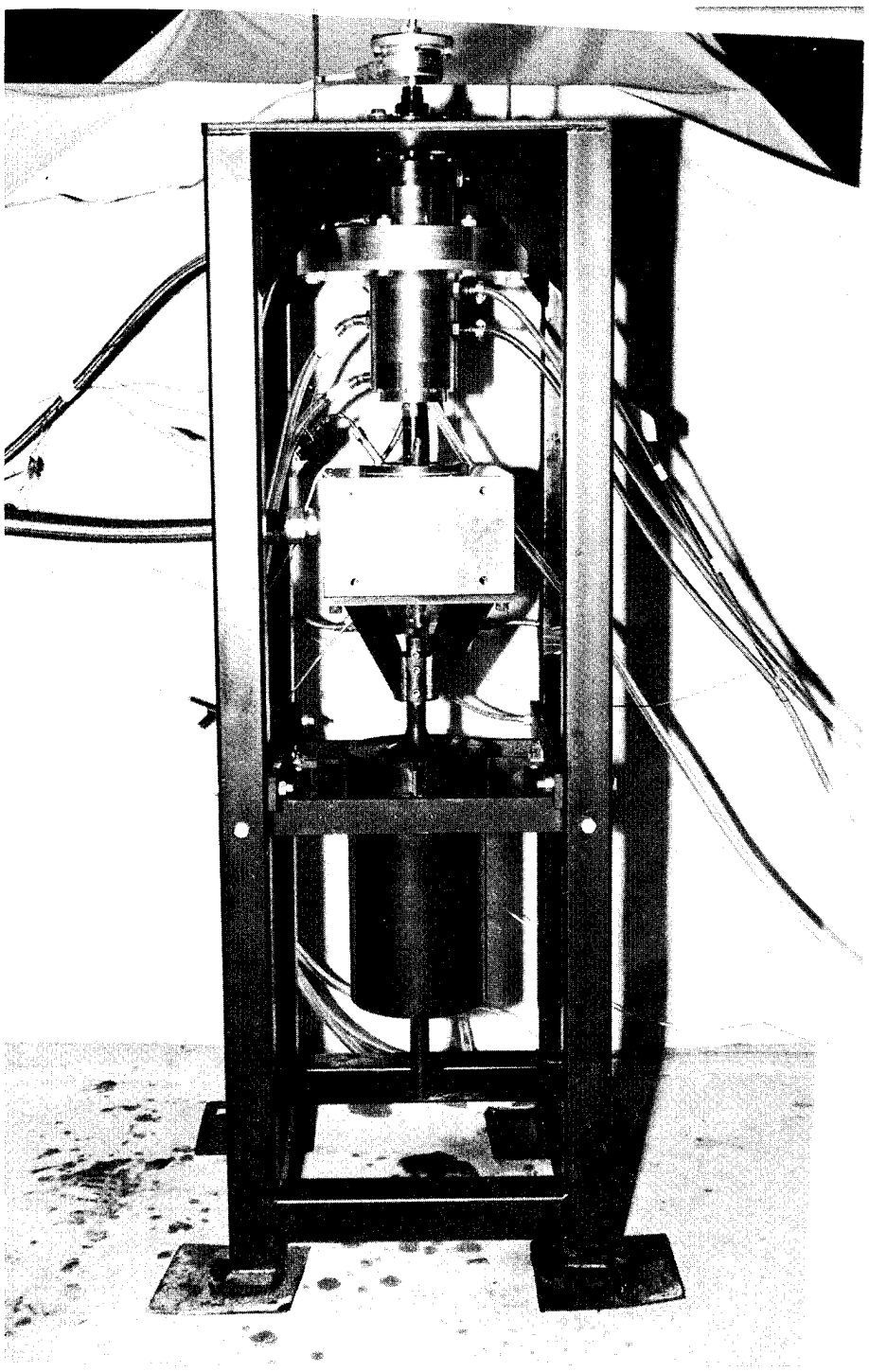

FIGURE 3-6

TEST SETUP

friction bearing. Rotation of the housing was prevented by a Lebow Model 2105-100 reaction torque sensor, thus measuring the total drag torque of all bearings and seals in the housing on any given run. A Barbour-Stockwell Model 6051 air turbine plus additional ballast was freely suspended from the test shaft to provide 175 pounds of static weight on the test bearings, thus simulating the anticipated weight of a complete flywheel rotor. The turbine was used to drive the test shaft at any desired speed up to the maximum design speed of 41,000 rpm. In the test item itself, the 175 pound load was shared by all three bearings; however in the turbine, this same load was carried by a single bearing. This proved to be a serious problem as it limited the amount of time the system could dwell at high speeds without overheating this critical turbine bearing. Twice tests had to be shut down prematurely to replace turbine bearings.

Signals from the strain gage bridge in the torque sensor were conditioned by a Daytronic Model 870 strain gage conditioner-amplifier; tachometer signals from a magnetic pickup in the drive turbine were conditioned by a Daytronic Model 840 frequency to voltage converter. Both parameters were displayed on-line as X-Y recordings of drag torque versus shaft speed on a Hewlett Packard Model 7005B recorder.

Lubricant flow to each bearing was measured continuously by Brooks Model 1355-V-R6-15-A rotameters, which were calibrated with the Santotrac-30 lubricant prior to beginning the formal testing program. Lubricant temperatures into and out of each bearing were sensed by Type K thermocouple probes inplanted in the plastic tubing used to circulate the lubricant into and out of the test hardware. Temperature data was displayed on a Doric Model DS-520 digital thermocouple indicator. The roughing pump, fore pump, and diffusion pump from a Veeco Model MS-9 helium leak detector were all used to establish the vacuum levels required in the test hardware during various portions of the testing program. Vacuum and differential pressure measurements were made with an assortment of gages and manometers.

3.2 TEST PROCEDURES AND RESULTS

First, the test item was to be assembled without seals, and drag torque values recorded with the bearings working at atmospheric pressure. Next, the workhorse seal was to be added and drag torque recorded at atmospheric pressure and again with a partial vacuum of 5 psia in the housing. Then, the test seals were to be added, and the torque recorded at atmospheric pressure with $\Delta P = 0$ across the test seals, again with 5 psia in the housing with $\Delta P = 0$ across the test seals, and again with a hard vacuum between the test seals and 5 psia elsewhere in the housing ($\Delta P = 5$ psi). Correlation of the recorded data would then yield a breakdown of the individual components making up the total drag recorded for the complete hardware.

Barometric pressures were between 24.9 and 25.8 inches of mercury (test facility @ 4,500 ft. elevation) with ambient temperatures between $58^{\circ}F$ and $84^{\circ}F$. Torque versus speed data was recorded continuously; temperature and pressure data was recorded at speeds of 0, 10, 20, 30, and 41 krpm.

In testing the bearings without seals, the only significant problem was a tendency of the lubricant to overflow its exhaust ports, flooding the bearings and causing excessive drag torque. At the high flow rates used in the beginning (50 cc/min to each bearing), flooding was severe, and torque increased rapidly with speed. Thereafter the lubricant flow rates were kept below 20 cc/min, and stable repeatable performance was obtained. Average data from four runs representing a total running time of 61 minutes:

TABLE 3-1

BEARINGS ONLY

PRIOR TO FIRST TURBINE BEARING FAILURE

SPEED (KRPM)	0	10	20	30	41
TORQUE (OZ-IN)	0.5	1.5	2.1	2.3	2.5
POWER (WATTS)	0	11	31	51	76
$\triangle$T @ BRG. NO. 1 (^{O}F)	0	13	14	15	15
$\triangle$T @ BRG. NO. 2 (^{O}F)	0	17	22	34	35
$\triangle$T @ BRG. NO. 3 (^{O}F)	0	10	.2	18	19

NOTES:

Absolute pressure in bearing cavity of 12.2 psia.

Ambient temperature range from 67^{O}F to 68^{O}F.

Lubricant viscosity range from 33 cs @ 67^{O}F to 13 cs @ 103^{O}F.

Lubricant flow of less than 20 cc/min to each bearing.

$\triangle$T values are lubricant out minus lubricant in temperatures. Lubricant flow rates are approximate because they were below the effective range of the original flow measuring apparatus, which was later changed to obtain more accurate data.

A failure of the main bearing in the drive turbine was experienced on the last data run. The turbine bearing was replaced, the test item disassembled and visually inspected. No damage was reported, although we now suspect that the test shaft might have bent slightly at the time of the turbine bearing failure.

The original ferrofluidic workhorse seal was then installed, and its ability to hold a partial vacuum of 5 psia in the bearing cavity verified at zero speed. The shaft spun freely by hand, but high speed spin testing produced erratic torque measurements. Subsequent vacuum integrity at zero speed was still good; however disassembly and visual inspection revealed indications of rubbing contact between the shaft and the stationary pole blocks. Contact appears to have been caused

by shaft runout in the region of the seal. A labyrinth workhorse seal with a wider radial gap was then substituted, and stable performance obtained.

The only purpose of a workhorse seal was to permit maintenance of a partial vacuum in the bearing cavity. Since the labyrinth seal had no vacuum integrity at zero speed, and only partially sealed at speed, it was necessary to operate the vacuum pump continuously in order to maintain a partial vacuum in the bearing cavities. With the labyrinth workhorse seal in place, a significant breakaway torque (4.5 oz-in) at zero speed was observed. Also, torque increased with speed more rapidly than it had before. These higher torque values were found to be independent of the vacuum level maintained in the bearing cavities. The labyrinth seal was then removed, and the recorded torque was virtually the same, confirming that the increase was not caused by the labyrinth seal, nor was it related to the vacuum level maintained in the bearing cavity. We now believe it was caused by flexing of the bent shaft and the resulting radial loads on the bearings, as it diminished later in the program after the shaft was remachined.

TABLE 3-2

BEARINGS ONLY, ALSO
BEARINGS PLUS LABYRINTH WORKHORSE SEAL
AFTER FIRST TURBINE BEARING FAILURE

SPEED (KRPM)	0	10	20	30	41
TORQUE (OZ-IN)	4.5	7.5	8.0	9.5	10.0
POWER (WATTS)	0	55	118	211	303

NOTES:

Test duration insifficient for stabilized temperature rise measurements.

Absolute pressure in bearing cavity of 12.2 psia.

Ambient temperature range from 69^{o}F to 72^{o}F.

Lubricant viscosity range from 31 cs @69^{o}F to 12 cs @ 105^{o}F

Lubricant flow of 13 cc/min to each bearing.

The labyrinth seal was replaced, and the centrifugal test seals were installed using a fluorocarbon fluid having a magnetic saturation of 100 gauss. Any added torque due to seal drag was found to be unmeasurable, as the torque versus speed data was virtually the same as before:

TABLE 3-3

BEARING PLUS LABYRINTH WORKHORSE SEAL PLUS
CENTRIFUGAL TEST SEALS WITH 100 GAUSS FLUOROCARBON FLUID

SPEED	0	10	20	30	41
TORQUE (OZ-IN)	-	6.3	8.4	9.5	10.0
POWER (WATTS)	0	47	124	211	303
Δ T @ BRG. NO. 1 (^{O}F)	0	6	4	20	24
Δ T @ BRG. NO. 2 (^{O}F)	0	39	64	74	85
Δ T @ BRG. NO. 3 (^{O}F)	0	6	9	38	50

NOTES:

Absolute pressure in bearing cavity of 12.2 psia.
Absolute pressure in rotor cavity of 12.2 psia (ΔP = 0).
Ambient temperature range from 69^{O}F to 72^{O}F.
Lubricant viscosity range from 29 cs @ 71^{O}F to 5 cs @ 166^{O}F
Lubricant flow of 4 cc/min to Bearing No. 1.
Lubricant flow of 8 cc/min to Bearing No. 2.
Lubricant flow of 4 cc/min to Bearing No. 3.

From this, we have concluded that centrifugal seal drag was definitely less than 1.0 oz-in per seal at 41,000 rpm (30 watts per seal). The shaft was then spun to 40,000 rpm with ΔP = 0, then the cavity between the seals slowly evacuated to see if the seals could hold a partial vacuum of 10 in-Hg (ΔP = 5 psi). The seals failed at 9 in H-g(ΔP = 4.4 psi) by loss of magnetic fluid into the area between the seals. We have concluded that in their existing configuration, the centrifugal seals do not have adequate sealing integrity.

The workhorse seal was then removed, and drag torque (no fluid in the centrifugal test seals) was found to be only slightly less than recorded earlier, thus substantiating our earlier conclusion that centrifugal seal and labyrinth seal drag was very small.

The test housing and shaft were then remachined to accept the conventional test seals. They were installed with a fluorocarbon base fluid having a magnetic saturation of 100 gauss. Drag torque at 41,000 rpm was approximately 8 oz-in, which is less than that reported earlier with no seals at all. We believe this was due to the remachining and straightening of the shaft. We found these seals to have only a marginal ability to hold a hard vacuum against atmospheric pressure ($\triangle P$ = 12.7 psi) at zero speed. They failed completely when attempting to pull a vacuum while turning at 20,000 rpm. Upon disassembly, the top seal was found to be nearly dry, its fluid having blown into the vacuum area. The lower seal appeared to have remained intact. A drop in torque was recorded at the time the top seal failed. This, plus a correlation with data recorded later, has led us to believe that the seal drag at 41,000 rpm was approximately 2.3 oz-in per seal (70 watts), which is acceptable for this program.

A diester base fluid with a magnetic saturation of 450 gauss was then loaded into the conventional seals. Drag torque was virtually the same as with the fluorocarbon fluid over the entire speed range. At zero speed, the seals held a hard vacuum ($\triangle P$ = 12.5 psi) indefinitely; they held for a 30-minute dwell at 20,000 rpm, but failed at 40,000 rpm. Again, failure was found to be the top seal blowing into the vacuum area; the bottom seal remained intact. New fluid was added, and the sequence repeated with virtually identical torque data (70 watts per seal @ 41,000 rpm with $\triangle P$ = 0). This time the seal failed to hold a vacuum at 38,500 rpm.

TABLE 3-4

BEARINGS PLUS LABYRINTH WORKHORSE SEAL PLUS
CONVENTIONAL TEST SEALS WITH 450 GAUSS DIESTER FLUID
PRIOR TO SEAL FAILURES @ 38,500 and 40,000 RPM (TWO RUNS)

SPEED (KRPM)	0	10	20	30	41
TORQUE (OZ-IN)	3.8	6.8	8.1	8.2	8.3*
POWER (WATTS)	0	50	120	182	252*

* Extrapolated from 40 krpm

NOTES:

Test duration insufficient for stabilized temperature rise measurements.
Absolute pressure in bearing cavity of 12.5 psia.
Absolute pressure in rotor cavity of 1 micron ($\triangle P$ = 12.5 psi).
Ambient temperature range from $64^{O}F$ to $65^{O}F$.
Lubricant viscosity range from 30 cs @ $70^{O}F$ to 13 cs @ $103^{O}F$.
Lubricant flow of 5 cc/min to Bearing No. 1.
Lubricant flow of 10 cc/min to Bearing No. 2.
Lubricant flow of 5 cc/min to Bearing No. 3.

Composite plots of total drag torque versus shaft speed are presented in Figure 3-7 for the following conditions:

Bearings only.
Bearings plus conventional seals - both seals intact.
Bearings plus conventional seals - one intact and one dry.

These curves represent the smoothed mean of all raw data recorded under the conditions indicated. Tolerance bands are shown to indicate typical data scatter observed during these tests. The difference between the two upper curves represents the estimated drag of each seal; the estimated drag of all three bearings remains the same as that reported prior to the first turbine bearing failure and subsequent damage to the test shaft. If new hardware of the exact same design were fabricated and tested, we would expect the following performance:

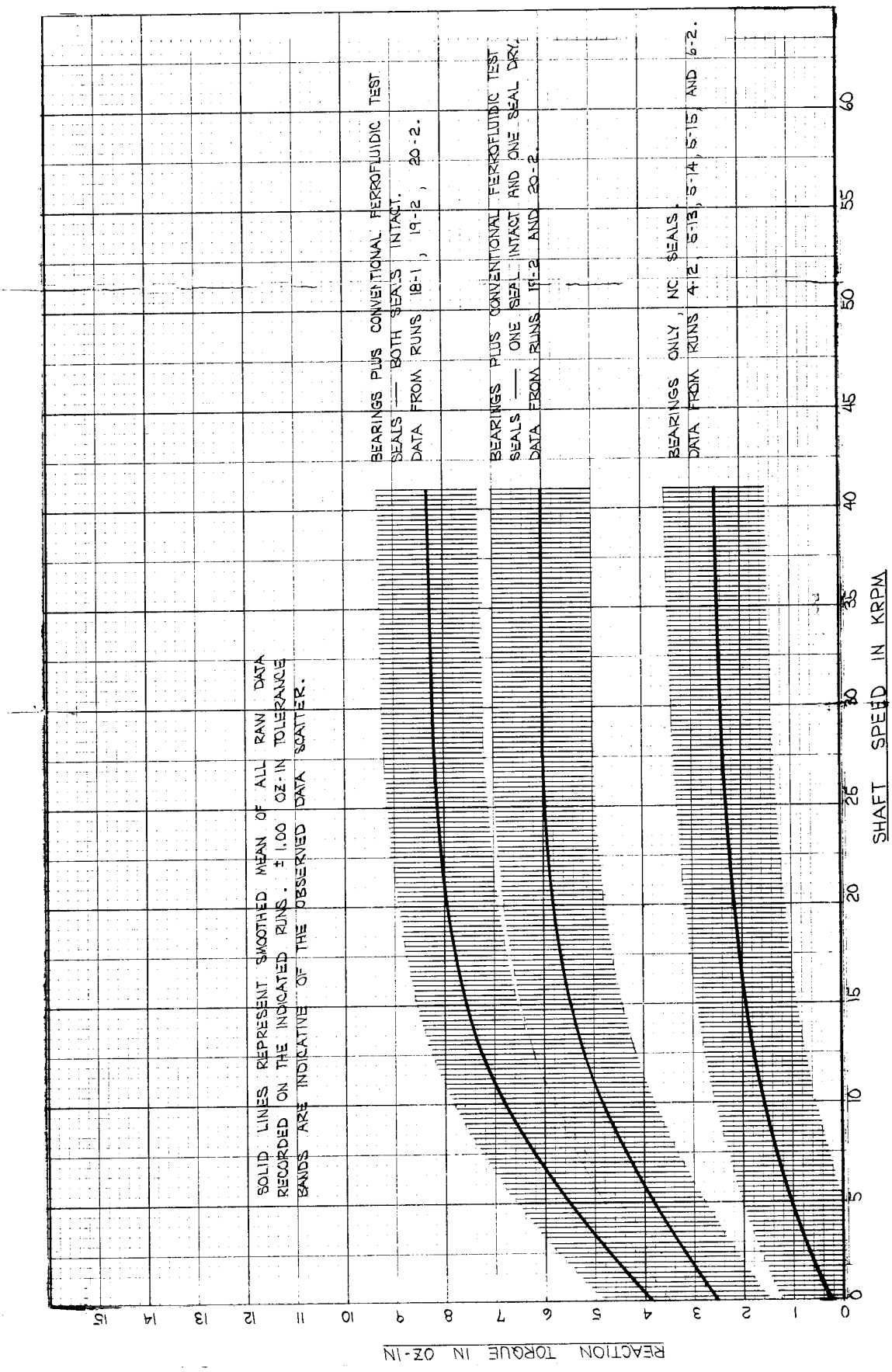

FIGURE 3-7

TORQUE VS. SPEED CHARACTERISTICS

TABLE 3-5

FINAL PERFORMANCE ESTIMATE
BEARINGS PLUS CONVENTIONAL SEALS

SPEED (KRPM)	0	10	20	30	41
DRAG OF 3 BEARINGS (OZ-IN)	0.5	1.5	2.1	2.3	2.5
DRAG OF 2 SEALS (OZ-IN)	2.6	4.0	4.4	4.5	4.6
TOTAL DRAG (OZ-IN)	3.1	5.5	6.5	6.8	7.1
TOTAL DRAG (WATTS)	0	41	96	151	215

3.3 POST-TEST ANALYSIS

A total of slightly over eleven hours of running at speeds between 10,000 and 41,000 rpm were logged on the bearings. Post-test inspection under 40X magnification showed orbital tracks of a dull finish on the individual balls in all three bearings, a normal condition for angular contact bearings running under heavy thrust loads. No other evidence of wear was found. We have concluded that bearing performance was satisfactory. The Santotrac-30 lubricant performed extremely well; however the pressurized jet distribution system was found to deliver excessive quantities to the bearings. It now appears that a wick feed air-oil mist system would be adequate.

Performance of the ferrofluidic centrifugal seals was unsatisfactory as they lacked the ability to withstand adequate pressure differentials. However, their drag torque was quite low and it appears that their sealing capabilities could be improved by the use of a larger slinger with radial grooves and a closer fit to the pole block on the low pressure side. This would improve the slinger's pumping function and thus improve its ability to hold pressure.

Performance of the conventional ferrofluidic seals was marginal; 70 watts per seal @ 40,000 rpm is acceptable, however better sealing integrity is needed above 38,000 rpm to meet the requirements of this program. This could be accomplished by adding more stages, using a different focusing structure on the shaft and/or pole blocks, using larger magnets or fluids of higher magnetic saturation, or by better isolation of the flux carrying circuit from other magnetic materials in the housing.

Maintaining a partial vacuum in the bearing cavities has proven to yield very little reduction in drag torque. Future testing will therefore be done with the bearings at atmospheric pressure, thus eliminating the need for a workhorse seal. Sealing of the test seals at zero speed is highly desirable as it minimizes contamination of the vacuum equipment and allows seal integrity checks prior to and upon completion of each test run.

One interesting concept is the possibility of combining the conventional and centrifugal seals into a hybrid unit as shown in Figure 3-8. At zero speed, the magnetic fluid would be concentrated in the region of the focusing structure on the low pressure side of the slinger. As such, it would seal in the same manner as conventional ferrofluidic seals. At high speeds, the pumping action of the slinger would tend to move the fluid outward and away from the focusing structure, thus minimizing the viscous shear (and torque) experienced in the narrow gap between the slinger and focusing structure. Sealing would then be accomplished as a classical slinger seal. Even if residual fluid trapped in the region of the focusing structure were to evaporate due to local heating, the vapor would tend to be pumped radially outward and be trapped by the liquid at the tip of the slinger. Whenever the speed is reduced, atmospheric pressure from the bearing cavity would force the fluid back into the focusing structure where it would again form a conventional ferrofluidic seal.

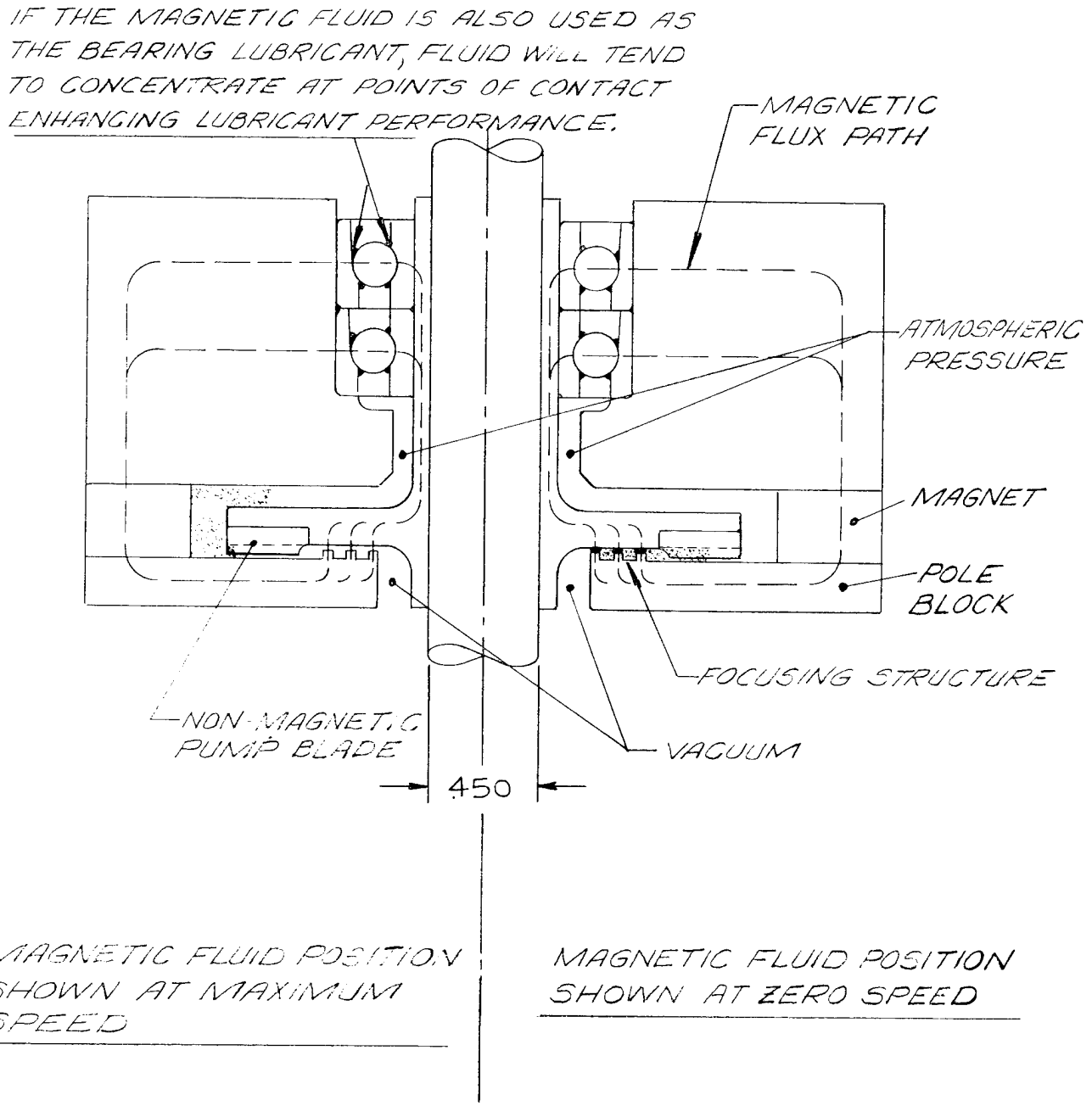

FIGURE 3-8

HYBRID SEAL CONCEPT #1

Another possibility to be considered is the use of a variable geometry slinger as shown in Figure 3-9. Here, a thin flexible member would be positioned to contact the pole block at zero speed, creating a ferrofluidic seal with an effective gap of zero. At speed, centrifugal forces would flex this member away from the pole block, up against the rigid slinger. The unit would then behave as a slinger seal in the manner described above.

For second generation hardware, a unitized bearing/seal cartridge is recommended. This would combine a duplex pair of bearings and the seal on a short hollow shaft with a self-contained wick feed or magnetic lubrication system something like that shown in Figure 3-10. Use of such a cartridge, regardless of the final seal configuration, would simplify assembly, produce greater shaft rigidity, and permit better control of the critical seal clearances.

Another problem that occurred during the test program was premature failure of the main bearing in the drive turbine, which was carrying the total thrust load of 175 pounds. Future testing should be conducted with a single bearing/seal cartridge at a thrust load of 90 pounds or less. This will allow testing at maximum speed for longer periods of time without overheating the main turbine bearing.

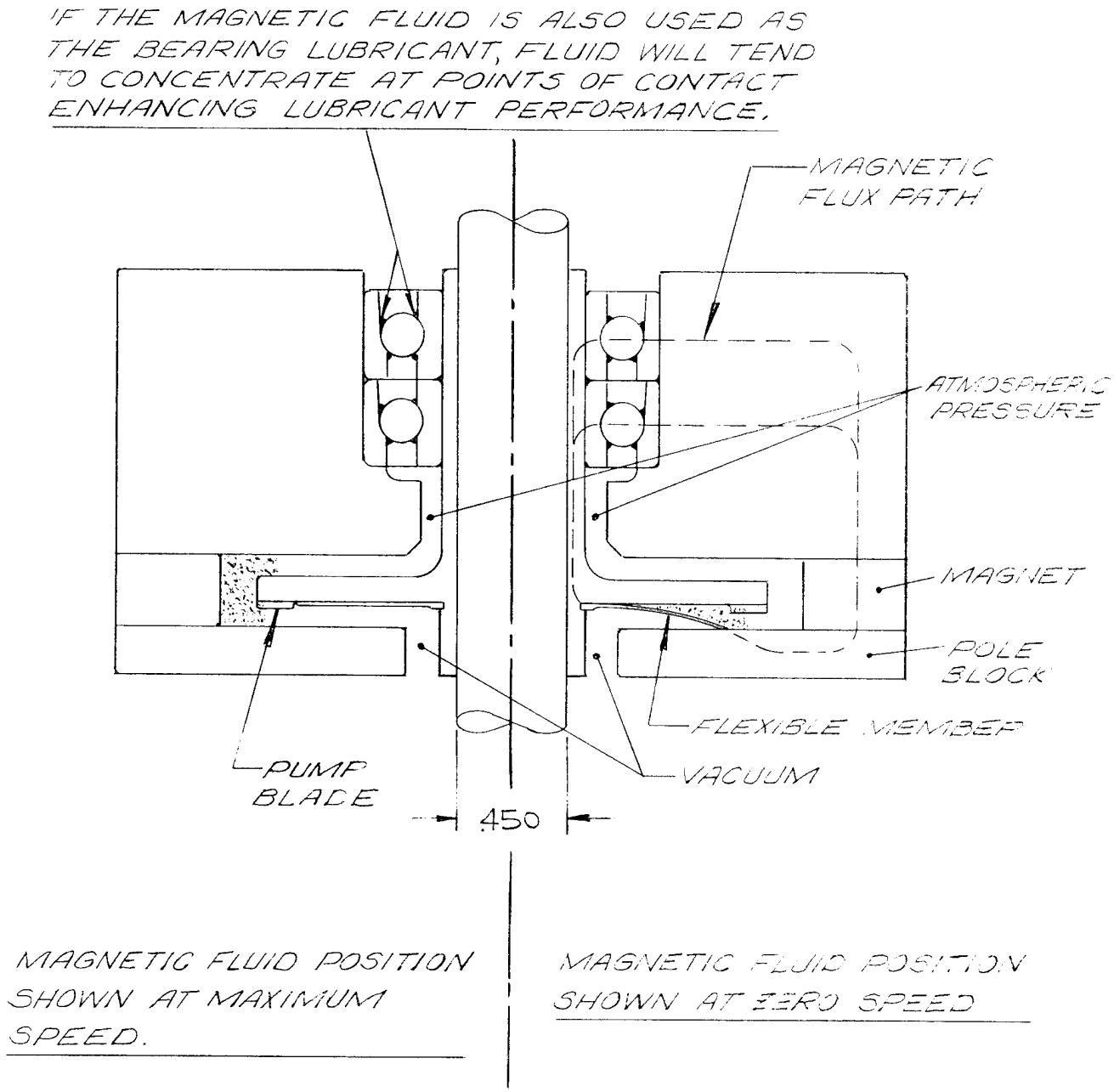

FIGURE 3-9

HYBRID SEAL CONCEPT #2

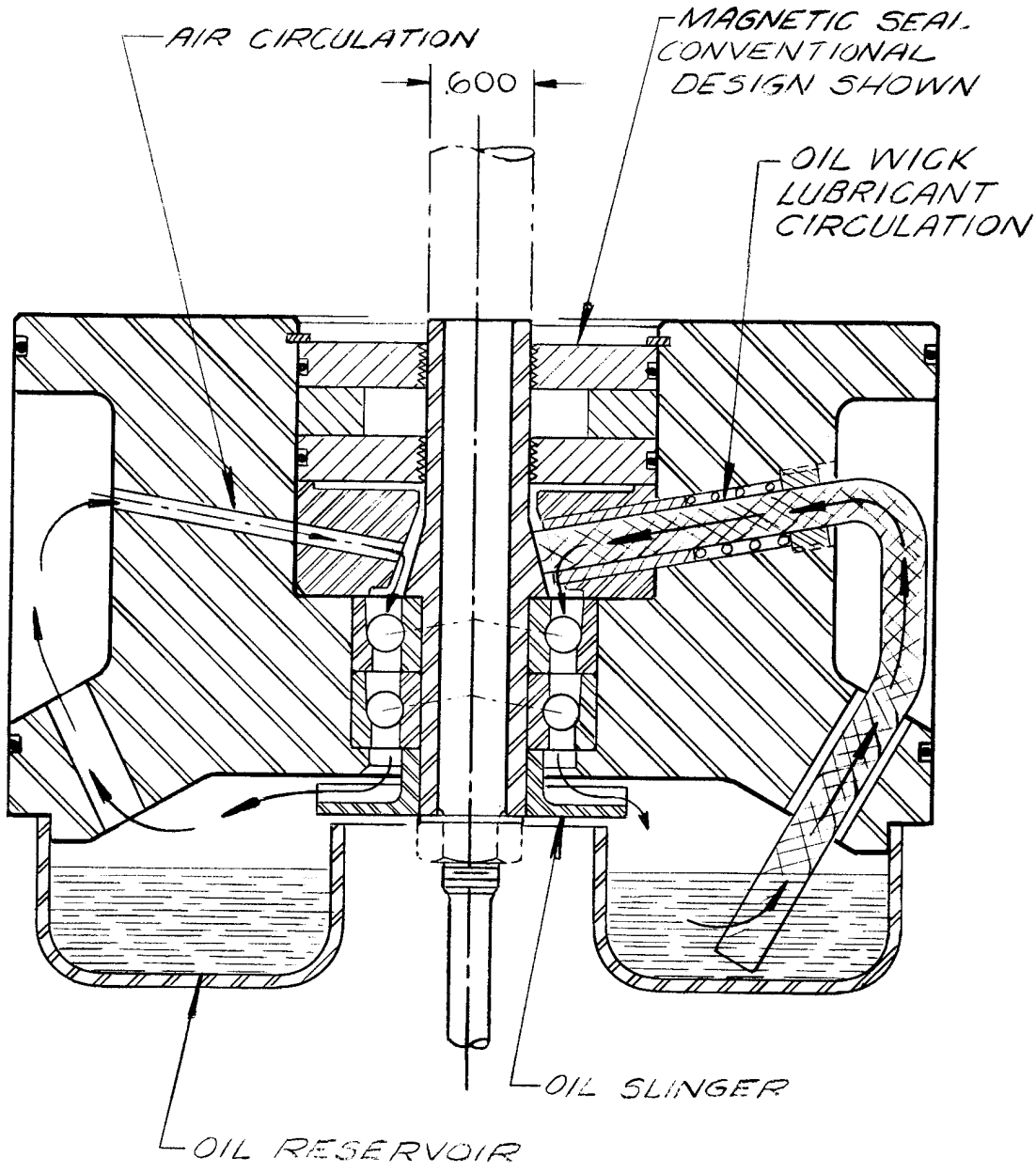

FIGURE 3-10

BEARING/SEAL CARTRIDGE CONCEPT

4.0 CONCLUSIONS

Even though the original goals of this program were not fully met, substantial progress was made. The problem areas are better defined, and practical solutions appear to be within grasp. Specific conclusions are:

a) Winding and curing full-size rims of apparent high quality was not as difficult as anticipated. Static strengths in excess of 250 ksi were reported from the NOL ring tests. Dynamic strengths in excess of 280 ksi are anticipated.

b) The rigid spoke/elastic attachment method of supporting test rims was dynamically unstable, and this was the primary reason the rotor program did not approach target speeds. As a result, the ultimate strength of full-size composite test rings under centrifugal loading conditions remains unknown. Spin testing to the ultimate speed capability of the composite itself is needed, and an alternative spoke system that will allow such speeds to be reached is proposed in the Recommendations section of this report.

c) Parasitic losses in test bearings and seals were very close to anticipated values, and a major effort to reduce them further does not appear to be warranted at this time.

d) The test results indicate that angular contact ball bearings may be adequate for near-term automotive flywheel systems, as the life projections for such bearings have been partially confirmed by the low drag torque and lack of perceptable wear observed over the short testing period. Longer testing periods are definitely needed to confirm bearing life projections.

e) A pressure fed bearing lubrication system should not be necessary, nor should maintenance of a partial vacuum in the bearing housings. A wick fed air-oil mist system operating at atmospheric pressure is a promising method for second generation hardware. For smaller rotors operating with less thrust load bearings using low vapor pressure synthetic greases operating in the vacuum are a distinct possibility. This would eliminate the need for high speed shaft seals altogether.

f) Only marginal sealing integrity was obtained from the two variations of ferrofluidic shaft seals tested. However, several design changes have been examined that very likely could improve their integrity.

Although the automotive energy storing flywheel using composite rotors concept was not proven to be clearly feasible, neither was it proven infeasible. The failure to meet program objectives thus far is traceable to inadequate design of test equipment and marginal seal performance. Solutions to these problems appear to be available, thus permitting the additional testing necessary to properly evaluate the composite rotor concept itself.

5.0 RECOMMENDATIONS

In view of the current interest in hybrid vehicles using battery-flywheel or heat engine - flywheel powerplants, LMC recommends this program be restructured to concentrate on development of smaller fly wheels suitable for use in such vehicles. Safety considerations favor the use of composite rotors. Such flywheels would generally have energy storage requirements in the range between 0.2 and 1.0 KW-HR. A family of single rim flywheels, each having the same inside diameter and axial length as the test rims developed in Phase I would be appropriate for this purpose. All could be filament wound with existing tooling, the only variable being the outside diameter. Thus LMC recommends that Phase II of this program address the task of demonstrating improved seal designs and a viable single rim rotor. Subsequent phases could ultimately lead to development of a family of composite flywheel packages for use in all manner of hybrid vehicles. A conceptual sketch of such a unit is presented in Figure 5-1.

A nylon or glass/epoxy torque ring on the inner surface applies compressive radial forces to the rim, thus reducing tensile radial stresses in the rim and thereby allowing use of a thicker section than would otherwise be possible. The "Small Rim Configuration" shown in Figure 5-1 represents a design of conservative radial thickness; the "Large Rim Configuration" represents a practical maximum in radial thickness. Early prototypes would be made thin to minimize the danger of radial delamination failures. Successive units could then be wound with larger and larger outside diameters until radial delamination problems begin to occur.

The most promising shaft-to-rim design known to LMC Corporation at this time is the "tension balanced spoke" concept presented by William M. Brobeck & Associates in their published report EPRI EM-227 (Reference 7). Such a system has already seen some laboratory testing, appears to be light-weight and inexpensive, yet rugged enough for service in automotive applications. Development would most likely proceed along these lines.

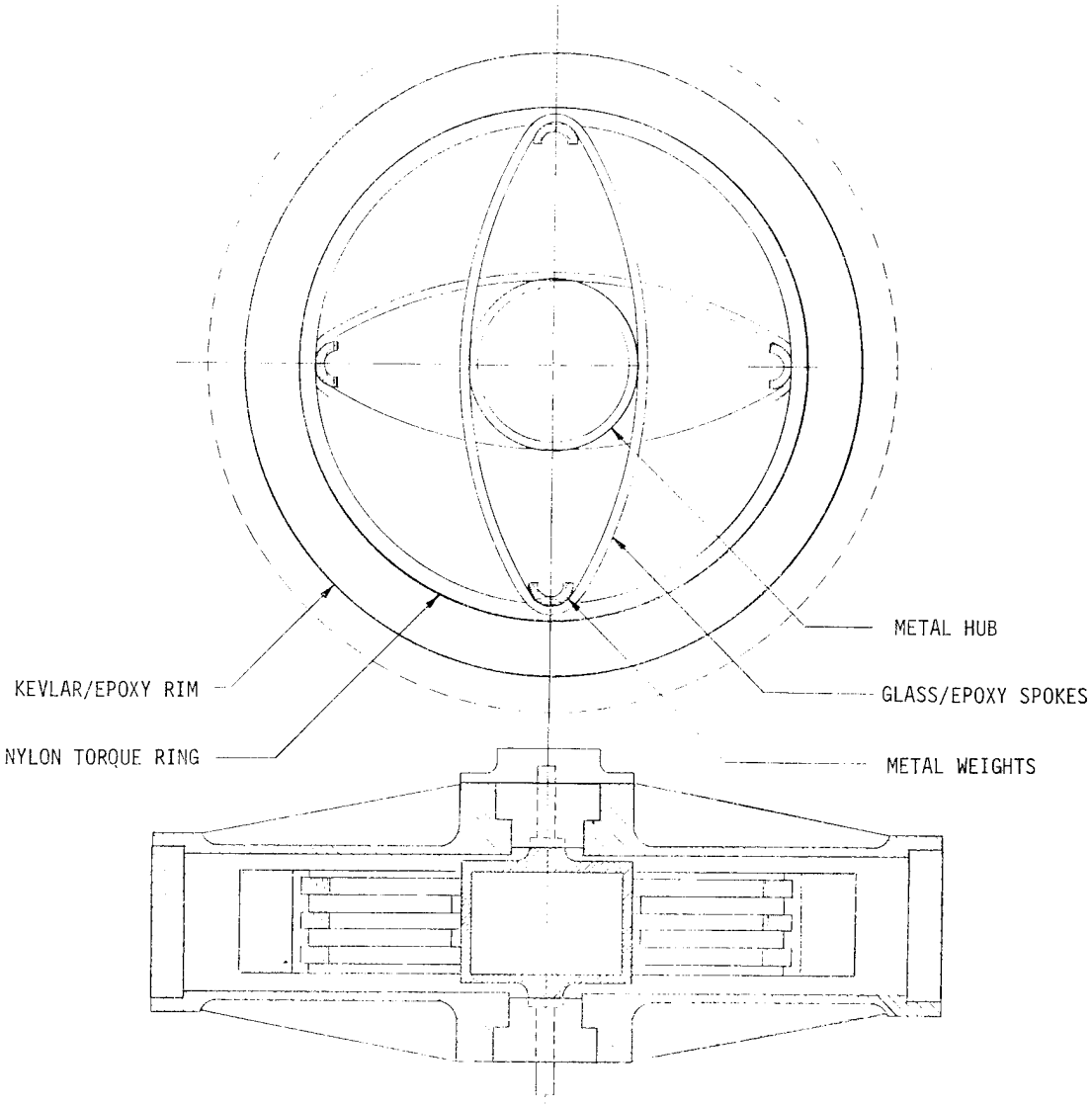

ULTIMATE SPEED CONDITION:

N = 46,900 RPM
S_H = 279,400 PSI (MAX)
S_R = 840 PSI (MAX)
KE = 947 W-H
KE/W = 63.9 W-H/LB
KE/W = 11.2 W-H/LB

SMALL RIM CONFIGURATION

ROTOR WEIGHT ----------14.8 LBS
TOTAL SYSTEM WEIGHT ---------84.8 LBS
OVERALL SIZE -------23" DIA X 9" HIGH

CONSERVATIVE SPEED RANGE:

N - 18,800 TO 37,600 RPM
S_H = 180,000 PSI (MAX)
S_R = 540 PSI (MAX)
KE = 457 W-H
KE/W_R = 30.9 W-H/LB
KE/W_S = 5.4 W-H/LB

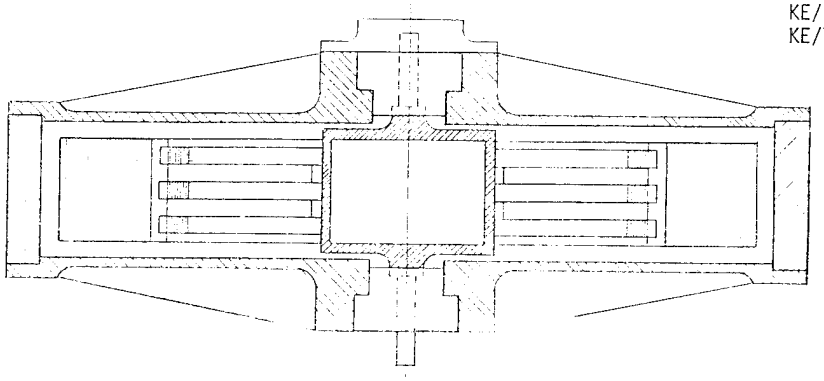

ULTIMATE SPEED CONDITION:

N = 38,500 RPM
S_H = 270,600 PSI (MAX)
S_R = 4,000 PSI (MAX)
KE = 1214 W-H
KE/W_R = 51.0 W-H/LB
KE/W_S = 12.9 W-H/LB

LARGE RIM CONFIGURATION

ROTOR WEIGHT ----------23.8 LBS
TOTAL SYSTEM WEIGHT ---------93.8 LBS
OVERALL SIZE ------23" DIA X 9" HIGH

CONSERVATIVE SPEED RANGE:

N = 15,700 to 31,400 RPM
S_H = 180,000 PSI (MAX)
S_R = 2,660 PSI (MAX)
KE = 606 W-H
KE/W_R = 25.5 W-H/LB
KE/W_S = 6.5 W-H/LB

FIGURE 5-1

PROPOSED WORKHORSE FLYWHEEL ASSEMBLY

APPENDIX A

REFERENCES

REFERENCES

1. Lear Motors Corporation; Demonstration of Near-Term Flywheel and Transmission Technologies Applied to an Automotive Propulsion System; Unsolicited Proposal LMC-300035 submitted to the Energy Research and Development Administration; April 30, 1975.

2. Lear Motors Corporation; Questions and Answers Relating to Proposal LMC-300035; submitted to the Energy Research and Development Administration; September 4, 1975.

3. USERDA and Lear Motors Corporation; Evaluation of Flywheel Drive Technology for a Commuter Car; Contract No. E(04-3)-1164; December 17, 1975.

4. Lear Motors Corporation; Spin Testing of Individual Rotor Elements; Test Procedure LMC-760301-B; May 26, 1976.

5. Lear Motors Corporation; Spin Testing of High-Speed Bearings and Seals; Test Procedure LMC-760302-B; May 12, 1976.

6. LMC Corporation; Spin Testing of Flywheel Bearings and Seals; Test Report LMC-760901-A; September 30, 1976.

7. Brobeck & Associates; Investigation of Multi-Ring Fiber-Composite Flywheels for Energy Storage; Final Report EPRI EM-227 (Research Project 269-2) prepared for the Electric Power Research Institute; September, 1976.

APPENDIX B

ROTOR DYNAMICS ANALYSIS

Prepared By

Dr. Charles N. McKinnon, Jr.
Program Manager

U. S. Flywheels, Inc.
1882 McGaw Avenue
Irvine, California 92714

DYNAMICS OF PENDULUS ROTORS WITH SPOKES CONNECTING HUB AND RIM

The failure of our flywheel systems to achieve target speed has prompted a review of the applicable dynamic relations. The case of a "rigid" flywheel/hub assembly, pendulously mounted, has been reviewed by Younger and Thomson in Ref. 1. The results of that study indicate that shaft whip is a limiting condition and the shaft first critical frequency must be above twice the desired operating speed. The shaft critical involved is that of a clamped-free end condition due to the stabilizing (clamping) effect of the disk when operating at high speed. Excitation for the shaft whip can be provided by a stable forward whirl mode resonance at twice spin speed, which yields one stress cycle of the shaft per spin revolution.

To elucidate this phenomena on our system, calculations were performed using our system parameters on the model of Ref. 1. Spin-whirl maps were prepared for both "A" and "L" systems. Important facts emerged when comparing the resulting theory with our actual runs:

1. The first critical shaft-whip frequency is definitely high enough so the failures cannot be attributed to shaft whip acting alone.
2. All of the failures occur during passage of the 2 times spin forward resonance pt. ($\sim$6000 rpm for L, $\sim$10,000 rpm for A).
3. When running steel ware only, or a rigid "dummy" disk, no problems were encountered passing the above frequencies.

The only plausible failure mode consistent with the above is a whip-like instability involving not only the shaft, but the shaft/hub/spoke combination; which is of a lower frequency than the exciting 2 x spin forward whirl. The following calculations result in a model that accounts for spoke finite stiffness in connecting the shaft and hub to the rim.

The basic model considered is shown in Fig. 1. The quill is considered clamped at the exit from the turbine section of the Barbour-Stockwell turbine and likewise at the shaft end. The effect of additional distributed masses which are part of the Barbour-Stockwell damping assembly are ignored. The effect of notching the quill near the shaft connection is neglected but can be easily accounted for by slight changes in the proper influence coefficients.

The shaft is clamped to the hub and is considered infinitely stiff. Its mass and moment of inertia are included in that of the hub. Likewise, the spoke mass and inertia contributions are included with the hub; the spokes are clamped to the hub but considered pinned at the rim and only the aggregate rotational spring constant is considered as the coupling between hub and rim. The transverse spring rate between hub and rim is considered infinite. This allows eliminating one degree of freedom, i.e., both rim

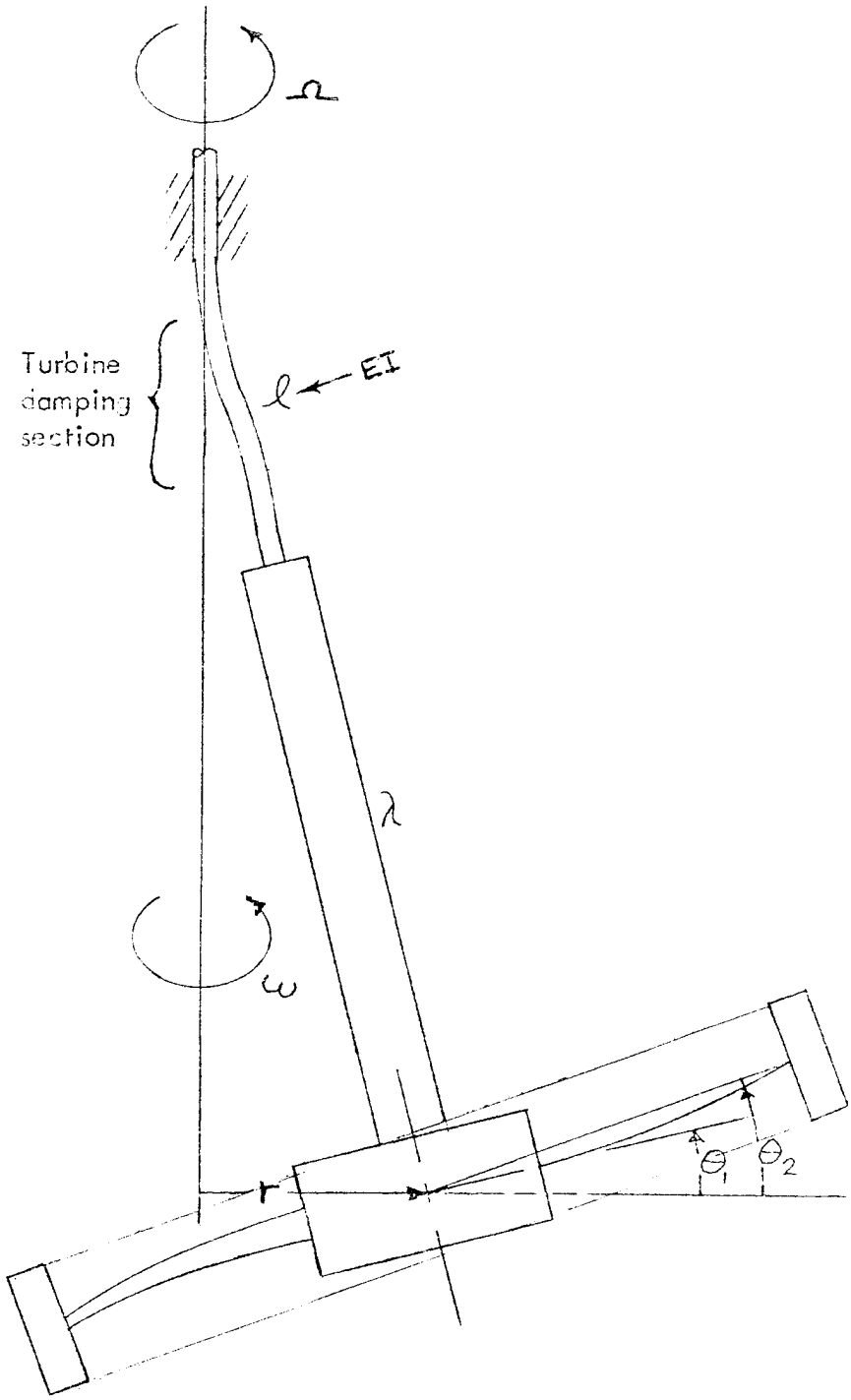

FIGURE 1: ROTOR Configuration Analyzed.

Assembly is undergoing steady spin, Ω, and whirl, ω. Turbine quill ℓ is major flexible shaft component. Stiffness of section λ is 33 times that of ℓ. Θ_1 is absolute tilt angle of hub, Θ_2 is absolute tilt angle of rim. Rim and hub maintain same center which is displaced amount r_o.

and hub are displaced the same amount, r ; the rim has mass, and polar and diametral moments of inertia. The nonlinear effect of gravity is ignored. At the desired speeds neglecting this stabilizing effect only introduces about 1% error.

Following Ref. 1, the analysis attempts to determine the relationships for steady spin-whirl:

1. Are there steady state spin-whirl modes, in this case for a three degree of freedom system?
2. What are the particular frequency relations in terms of known system parameters and the mode shapes?
3. The stability requirements for each mode?

The system can be broken down into three components as in Figure 2, and the dynamical relations stated. The principle equation for the steady-state solution is:

$$\sum \vec{M} = \vec{\omega} \times \vec{H} \tag{1}$$

Where $\sum \vec{M}$ is the total moment acting on a particular body having polar moment of inertia J and diametral moment I (and ratio $\alpha = \frac{J}{I}$), $\vec{H}$ is the angular momentum vector, and $\vec{\omega}$ is the whirl angular velocity. Equation (1) expresses the fact that a moment is required to change the direction of the angular momentum vector even though the magnitude of $\vec{H}$ is constant.

In Figure 2-a, the shaft consists of flexible portion ℓ and stiff portion λ The shaft is undergoing spin Ω , and whirl ω , about the vertical axis as shown. In equilibrium the hub produces a force and moment on the massless shaft so that from strength of materials only one can write:

$$r = \alpha_{11} P_T - \alpha_{12} M_S \tag{2}$$

$$\theta_1 = \alpha_{12} P_T - \alpha_{22} M_S \tag{3}$$

where the influence coefficients are

$$\alpha_{11} = \frac{1}{EI}\left(\ell^3/3 + \ell^2\lambda + \ell\lambda^2\right) \tag{4}$$

$$\alpha_{12} = \frac{1}{EI}\left(\ell^2/2 + \ell\lambda\right)$$

$$\alpha_{22} = \frac{1}{EI}\left(\ell\right)$$

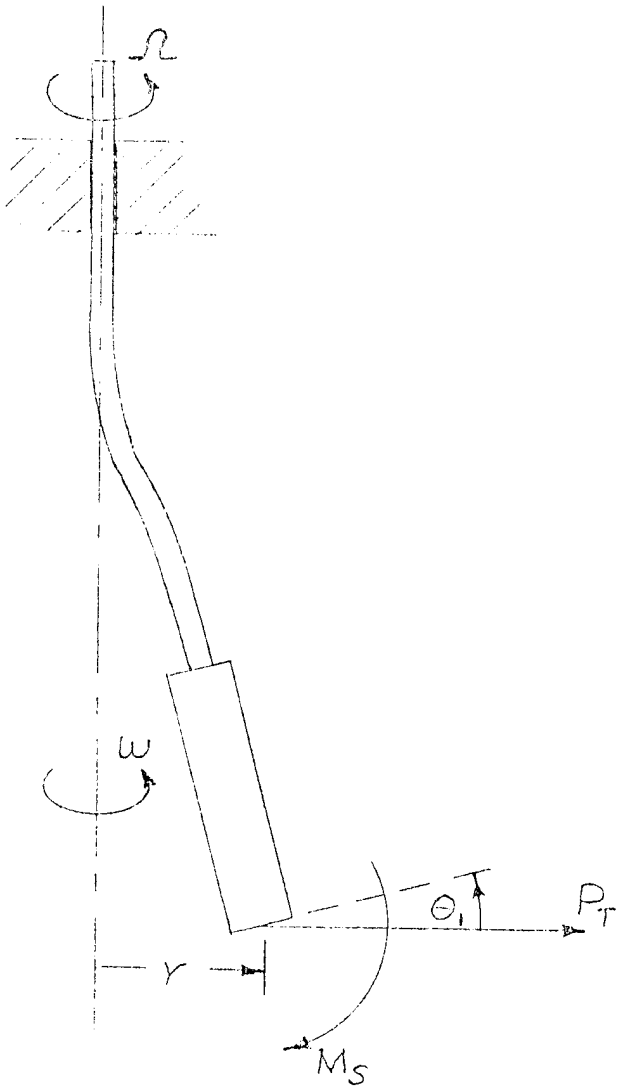

SHAFT/QUILL

Fig. 2a

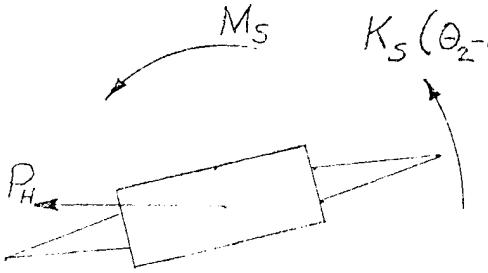

HUB/SPOKES

Fig. 2b

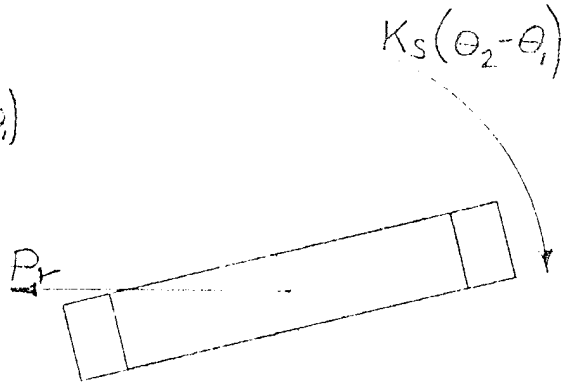

RIM

Fig. 2c

FIGURE 2:

Breakdown of Rotor assembly showing forces and moments on each component.

The hub shown in Figure 2-b is subject to the equal and opposite shaft force and moment, and, in addition, a moment from the spoke deflection ($\theta_2 > \theta_1$). Applying (1), along with the small angle approximation ($\sin\theta \cong \theta$, $\cos\theta \cong 1$) yields:

$$\omega\left(J_h \Omega - I_h \omega \right)\theta_1 = M_s + k_s\left(\theta_2 - \theta_1\right) \qquad (5)$$

Equilibrium of hub contribution of horizontal shaft force and hub steady centrifugal force gives:

$$P_h = m_h r \omega^2 \qquad (6)$$

For the rim shown in Figure 2-c there is likewise a force to balance the centrifugal force:

$$P_r = m_r r \omega^2 \qquad (7)$$

and the rim moment equilibrium

$$\omega\left(J_r \Omega - I_r \omega \right)\theta_2 = -k_s\left(\theta_2 - \theta_1\right) \qquad (8)$$

(6) and (7) can be combined with (2) to yield:

$$P_T = P_r + P_h = m r \omega^2 \qquad (9)$$

where m is now the total system mass.

When (9), (8), (5) are substituted into (2) and (3) and written in standard matrix form for the 3 degrees of freedom, homogeneous equations result:

$$\begin{bmatrix} (-k_s) & \left[\omega\left(J_r\Omega - I_r\omega\right) + k_s\right] & (0) \\ \left[1 + \alpha_{22}\omega\left(J_h\Omega - I_h\omega\right) + \alpha_{22}k_s\right] & \left(-\alpha_{22}k_s\right) & \left(-\alpha_{12}m\omega^2\right) \\ \left[-\alpha_{12}\omega\left(J_h\Omega - I_h\omega\right) - \alpha_{12}k_s\right] & \left(\alpha_{12}k_s\right) & \left(\alpha_{11}m\omega^2 - 1\right) \end{bmatrix} \cdot \begin{Bmatrix} \theta_1 \\ \theta_2 \\ r \end{Bmatrix} = 0 \qquad (10)$$

For non-trivial solutions, the determinant of (10) must equal zero, resulting in the frequency equation after some algebraic manipulation:

$$
\begin{aligned}
&-\alpha_{12}^2 m\omega^2 g_r g_h - \alpha_{12}^2 m\omega^2 g_h K_s - \alpha_{12}^2 m\omega^2 g_r K_s \\
&\alpha_{11} m\omega^2 g_r + \alpha_{11} m\omega^2 g_r g_h \alpha_{22} + \alpha_{11} m\omega^2 g_r K_s \alpha_{22} \\
&\alpha_{11} m\omega^2 K_s + \alpha_{11} m\omega^2 g_h K_s \alpha_{22} - g_r \qquad (11) \\
&-\alpha_{22} g_r g_h - g_r \alpha_{22} K_s - K_s - K_s \alpha_{22} g_h = 0
\end{aligned}
$$

where $$g_h = \left(a_h \frac{\Omega}{\omega} - 1\right)\omega^2 I_h \qquad (12)$$

and $$g_r = \left(a_r \frac{\Omega}{\omega} - 1\right)\omega^2 I_r \qquad (13)$$

The solution of (11) is facilitated if non-dimensional factors are introduced:

$$D_r = \frac{\alpha_{22} I_r}{\alpha_{11} m} \quad = \text{rim disk factor} \qquad (14\text{-a})$$

$$D_h = \frac{\alpha_{22} I_h}{\alpha_{11} m} \quad = \text{hub disk factor} \qquad (14\text{-b})$$

$$P_r = \frac{\alpha_{22} J_r}{\alpha_{11} m} \quad = \text{rim polar factor} \qquad (14\text{-c})$$

$$P_h = \frac{\alpha_{22} J_h}{\alpha_{11} m} \quad = \text{hub polar factor} \qquad (14\text{-d})$$

$$E = \frac{\alpha_{12}^2}{\alpha_{11}\alpha_{22}} \quad = \text{elastic factor} \qquad (14\text{-e})$$

$$R = K_s \alpha_{22} \quad = \text{spoke/quill stiffnes factor} \qquad (14\text{-f})$$

$$S = \frac{\Omega}{\sqrt{\alpha_{11} m}} \quad = \text{non-dimensional spin freq.} \qquad (14\text{-g})$$

$$F = \frac{\omega}{\sqrt{\alpha_{11} m}} \quad = \text{non-dimensional whirl freq.} \qquad (14\text{-h})$$

When the above substitutions are made in (11) the result is quadratic in S and 6th order in F:

$$a(F)S^2 + b(F)S + c(F) = 0 \qquad (15)$$

where

$$a(F) = P_r P_h \left\{ F^2 \left[F^2 (1-E) - 1 \right] \right\} \tag{16}$$

and

$$b(F) = F^5 (E-1)(P_r D_h + D_r P_h)/R + F^3 \left[(P_r D_h + D_r P_h)/R - E(P_r + P_h) \right] + F \left[(F^2 - 1)(P_r + P_h + P_r/R) \right] \tag{17}$$

and

$$c(F) = F^6 D_h D_r (1-E)/R + F^4 \left[(E-1) D_h - (1 + D_h) D_r/R \right] + F^2 \left[1 + D_h + D_r (1 + 1/R) \right] - 1 \tag{18}$$

Equation (15) and its auxillaries (16) - (18) are most easily solved by assigning a range of values for F, then calculating a, b, c; finally, the quadratic formula applied to (15) yields two real values of S for each assigned F.

A check on the accuracy of (16) can be made by letting $R \to \infty$, which corresponds to the rigid hub/rim in Ref. 1. Indeed, equation (15) reduces to

$$S = \frac{D(E-1)F^4 + (D+1)F^2 - 1}{\alpha F D \left[(E-1)F^2 + 1 \right]} \tag{19}$$

where $D = D_r + D_h$, and $a = \left(\frac{J}{I}\right)$, for the combined rim and hub assembly.

$$\frac{PR + PH}{IR + IH} = \frac{J}{I}$$

The numerical computations were performed on a Digital Equipment Corporation (DEC) System-10 computer via a straightforward FORTRAN program, a sample of which is shown as Figure 3. The Parameter R was assigned five values, to encompass the expected experimental values, in this case the half-decade increments 3.16, 10, 31.62, 100, 316.2. It should be mentioned that as various input parameters were calculated it was found that the hub diametral inertia is greater than the polar inertia ($AH = .7$) due mainly to the long stiff section $\overline{\lambda}$. In contrast the rim approaches a thin disc with $AR = 1.8$. The hub alone is then dynamically unstable. Only strong spoke coupling to the rim can provide for a possible stable system.

The input values in the program correspond to the "A" system parameters. A sample of the resulting spin-whirl maps are shown in Figures 4, 5, and 6. In these figures only the upper two branches are plotted. The third branch corresponds to the low frequency pendulus mode and lies entirely below the retrograde position of the lower branch shown. For $-\Omega > \omega$ it is unstable due to quill hysterisis and only external damping can provide the required bounded amplitudes. The lower section of the turbine housing does provide adequate damping for this mode. (See Figure 1).

Two major features stand out in the spin-whirl maps:

1) There is a crossing of the two upper branches; and as R increases, the branches diverge without crossing;

2) One branch crosses the S = F line at high spin and is thus potentially unstable. For AH greater than one, the branch would be stable and remain above the synchronous whirl line, S = F.

Time has not permitted evaluating all possible mode shapes θ_1/r, θ_2/r, θ_1/θ_2. However, the later ratio can easily be obtained from the top line of equation (15):

$$-K_s \underbrace{(D_r)}_{\theta_1} + I\omega(J_r\Omega - I_r\omega) + K_s\theta_2 = 0 \qquad (20)$$

This is non-dimensionalized by (14) to yield:

$$\theta_1/\theta_2 = \frac{F^2 D_r}{R}\left(A_r \frac{S}{F} - 1\right) + 1 \qquad (21)$$

setting $\theta_1/\theta_2 = 0$ yields:

$$S = \frac{1}{A_r}\left(F - \frac{R}{F D_r}\right) \qquad (22)$$

```
MAIN.   LN6EWN,FOR      FORTRAN V.4A(317) /KI   22-MAR-77

000001          E = .98
000002          AR = 1.8
000003          AH = .7
000004          DR = .06
000005          DH = .015
000006          DRB = DR * AR
000007          DHB = DH * AH
000008          D = DR + DH
000009          DB = DRB + DHB
000010           DRBDH = DRB * DH
000011          DHBDR = DHB * DR
000012          DO 10 J = 1,5
000013          AJ = .5 * (J-1) + .5
000014          R = 10. ** AJ
000015          PRINT20,R
000016    20    FORMAT(//,10X,'R = ',F7.2)
000017          B = (DRBDH + DHBDR) /R
000018          A1 = DHB * DRB /R
000019          B1 = DRB + DHB + DRB/R
000020          B2 =B - E*DB
000021          B3 = B*(E-1)
000022          C0 = 1. + D + DR/R
000023          C2 = D*(E-1) - DR*(1.+DH)/R
000024          C4 = DH*DR*(1-E)/R
000025          F = 75.
000026          DO 10 I = 1,150
000027          F = F + .5
000028          AA = A1 *(F*F*(1.-E)-1.)
000029          BB = B1*(F*F-1)/F + B3*F*F*F + B2*F
000030          CC = -1./F/F + C0 + C2*F*F + C4*F*F*F*F
000031          DISC = BB*BB - 4. * AA * CC
000032          IF(DISC.LT.0.0) GO TO 10
000033          RT1 = (-BB + SQRT(DISC))/2./AA
000034          RT2 = (-BB -SQRT(DISC))/2./AA
000035    620   PRINT60,F,RT1,RT2
000036    60    FORMAT(/,3X,F5.1,5X,2E10.3)
000037    10    CONTINUE
000038          STOP
000039          END

SUBPROGRAMS CALLED

SQRT.
```

FIGURE 3: FORTRAN program for calculating spin-whirl modes, eqn.(15) (16) (17) (18). The inner loop generates values of F, in this case from 75 to 150. The outer loop provides the half decade increments of R.

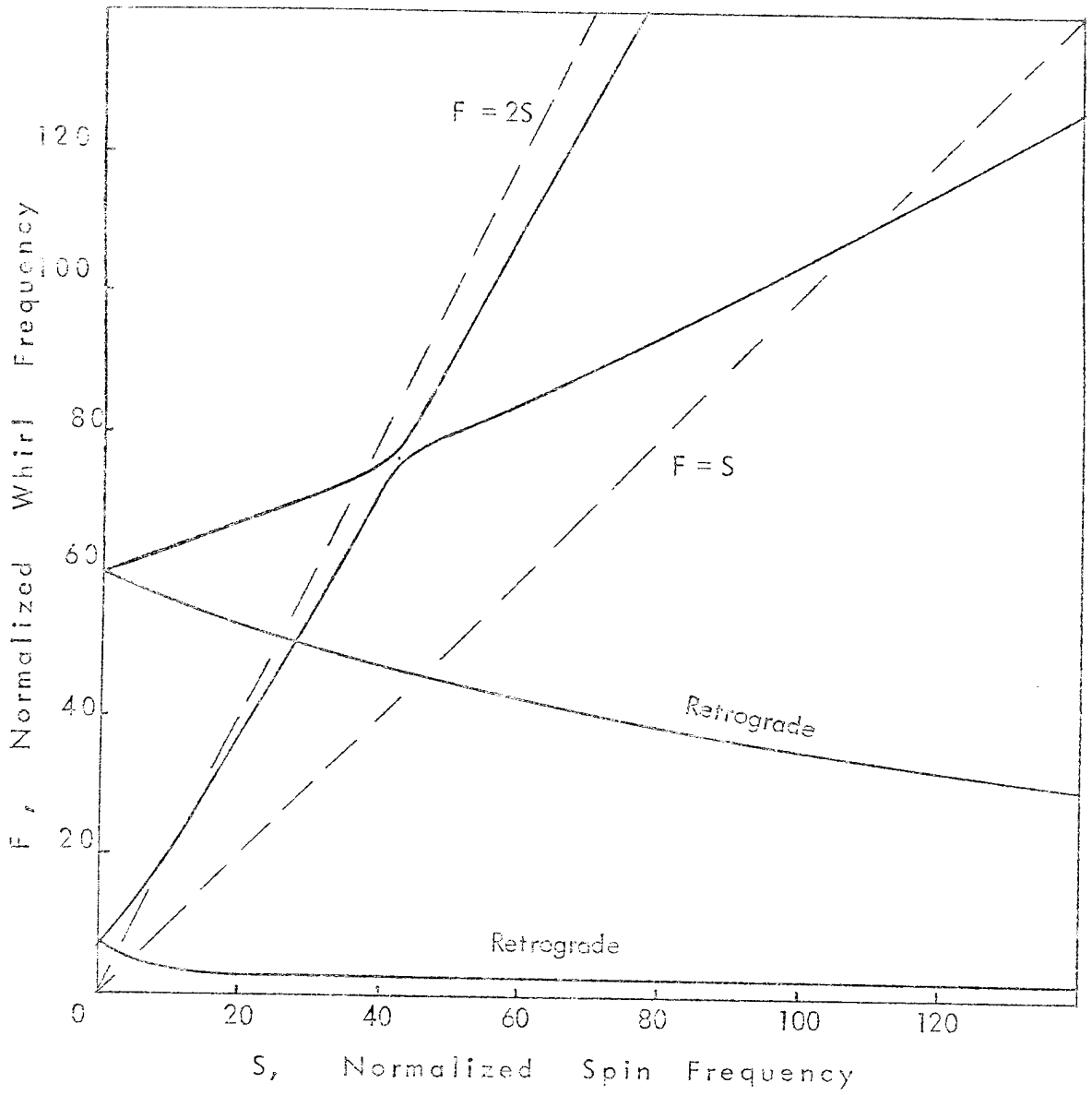

LN6 AND LN6EWP

FIGURE 4: Spin-Whirl map for R = 3.16.

From data of 22 March 77, LNGEWN E = .98,
D_r = .06, D_h = .015, A_r = 1.8, A_h = .7.
Multiply S and F values by 187 to obtain ω in RPM.

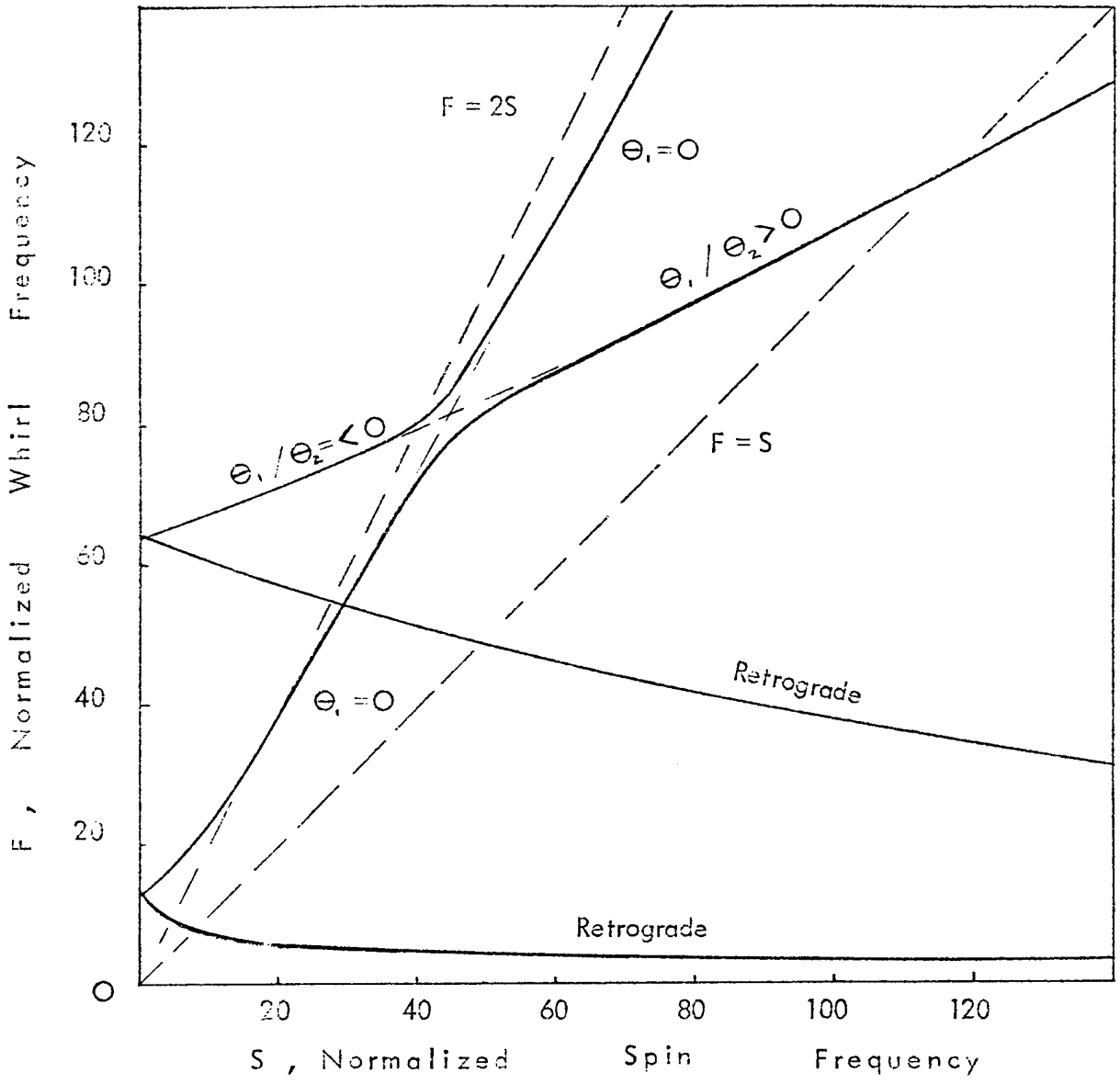

FIGURE 5: Spin-Whirl map for R = 10.0
Other data same as Figure 4.

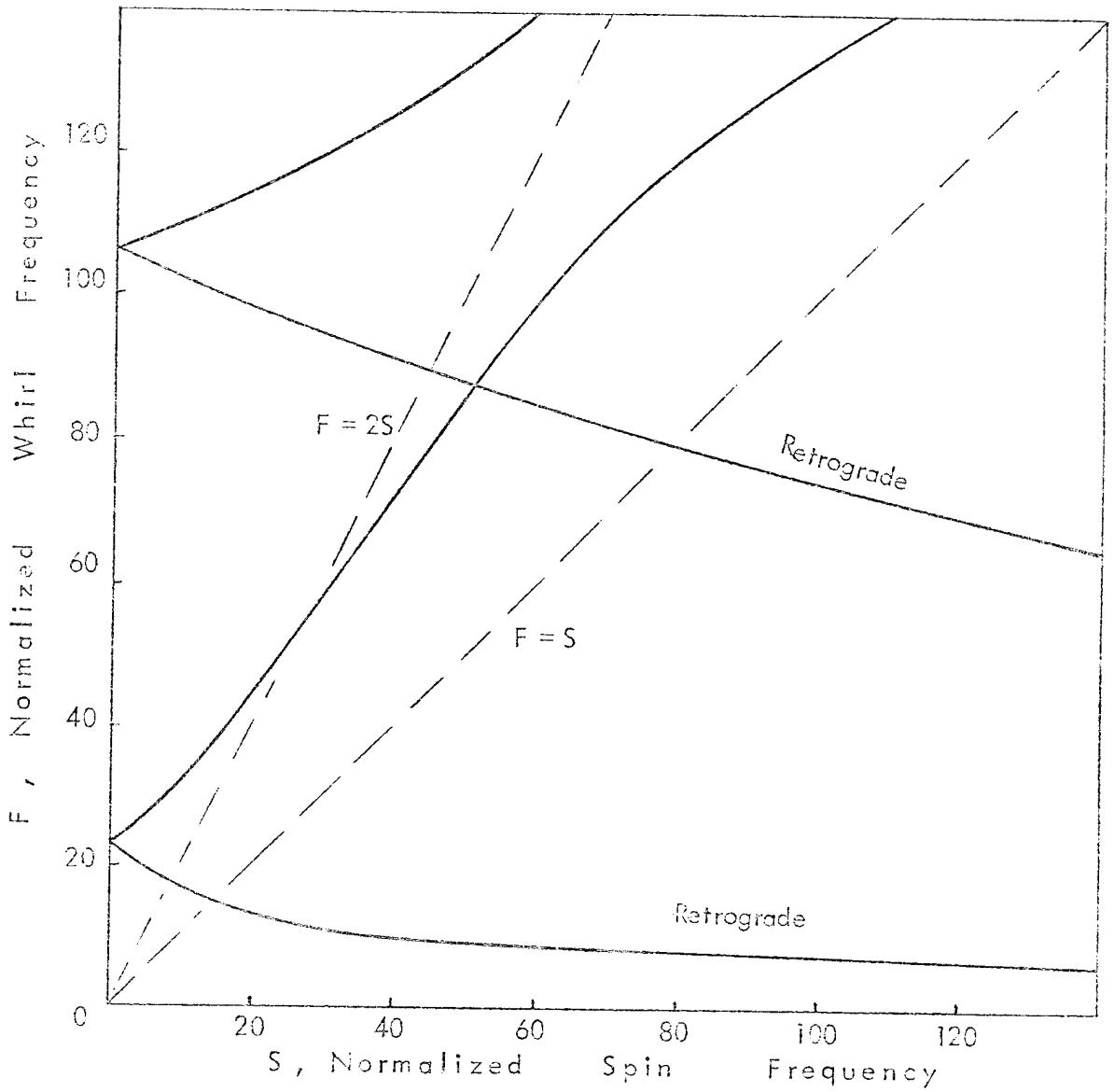

FIGURE 6: Spin-Whirl map for R = 100.0
Other data same as Figure 4.

This locus is exactly the branch that almost parallels the F = 2 S line. For instance, in Figure 5 where R = 10, well above and below the crossing, $\theta_1/\theta_2 = 0$, and as the crossing is approached θ_1/θ_2 takes finite values positive to the right and negative on the left, with greater ratios the further away from the intersection.

As the flywheel is run up in speed (increasing Ω), no resonances on the upper branch are observed at 5 X, 4 X, 3 X crossings because the large negative ratio of θ_1/θ_2 requires large spoke forces; for instance, at 4 X, $\theta_1/\theta_2 = -15.4$.

As the 2 X intersection is approached, the ratio of θ_1/θ_2 approaches zero. In other words, the coupling between rim and hub is loose, and spoke forces are low in the steady state deflection. This allows any hub vibration to be excited by the 2 X whirl resonance. Indeed, calculations show that the hub-shaft-quill combination has an unstable θ_1 motion at a frequency above the 2 X spin frequency but <u>less than</u> the 2 X whirl frequency.

The added hysterisis losses in the spokes from the θ_1 motion produces torsional forces on the hub to compound the already unstable vibration. The conclusion is that both stiffer spokes and proper polar ratios are needed for a stable system.

It can be seen by comparing figures 4, 5 and 6, that as R increases the spin frequency of the 2 X intersection increases in parabolic fashion so that R values of only about 300 are required to make the 2 X intersection above the desired spin operating frequency.

☆U.S. GOVERNMENT PRINTING OFFICE: 1978-740-094/1183